Universiteit Utrecht

2023-2024

MSc Thesis

How the Paleoclimate of the Younger Dryas Stadial influenced Sand Deposition in Pingo Remnants in the Northern Netherlands.

Author
Leonardo Bonanno
ID: 1280198

First Supervisor
Dr. W.Z. Hoek

Second Supervisor
Dr. T.H. Donders

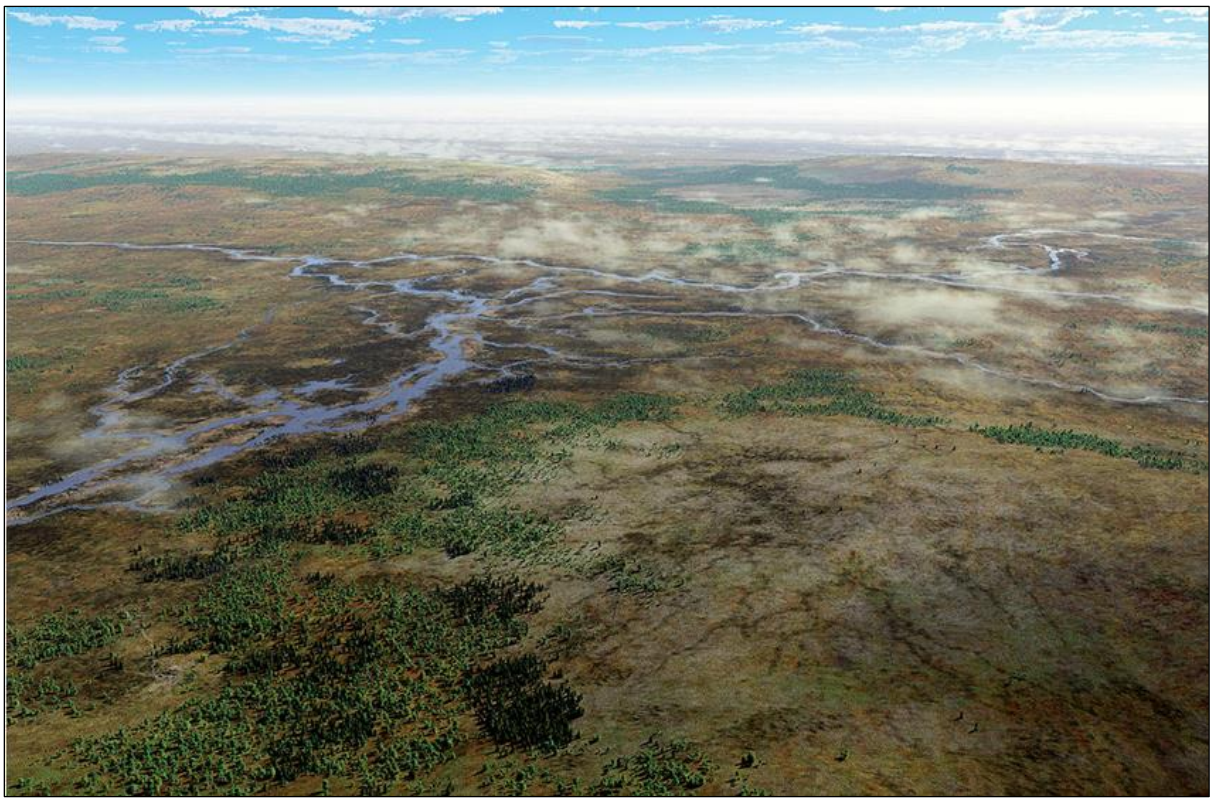

Figure 1. Artistic reconstruction of the Dutch landscape around approximately 10.000 BC during the Younger Dryas above Twente, Netherlands (Kriek, 2015).

Abstract

This research investigates the impact of the Younger Dryas stadial, a cold and windy period of the Pleistocene, on the aeolian sediments from the cores extracted in pingo remnants in the Northern Netherlands. Pingos are geomorphological features occurring during glacial periods and are characterised by hill-shaped ice lenses buried under the surface. When the ice melts, the structure collapses into a lake depression called pingo remnant which captures sediments until it dries up completely. By analysing the inorganic content from sediment cores extracted from four different pingo remnants, the study focuses on understanding the connection between aeolian sands and the climatic shifts that occurred in the Younger Dryas.
The main objective of the study is to identify the characteristics of the Younger Dryas sediments such as the organic content, sand/silt ratio, median sand grain diameter and sand grain heterogeneity. The methods consist of field work for collecting samples which are subsequently transferred to the lab for treatments and analysis. Samples of sediment were extracted from the cores, then dried, ashed, weighed, fractionated by grain size and photographed under the microscope.
The results of the study helps to understand better the role that the Younger Dryas played in affecting the vegetation cover, and distribution of aeolian deposits in the northern Netherlands. The conclusions suggest that there is a connection between the temperature, humidity and wind trends with the response seen in the vegetation cover and aeolian sediments. The fluctuations measured from the residuals of the Loss on Ignition treatment, the sand/silt ratio, median sand grain diameter and sand grain heterogeneity are interpreted as the consequences of a gradual increase in wind speeds throughout the Younger Dryas. The findings suggest that the highest wind speeds and lowest vegetation cover occurred at the end of this period, just before the abrupt onset of the Holocene, where temperatures increased dramatically again. Other observations of the results indicate that the organic content decreased steadily throughout the Younger Dryas, and it is correlated inversely with the sand to silt mass ratio from the inorganic portion of the sediments. The degree of sandiness from aeolian origin increased gradually, peaking just before the onset of the Holocene with a slight but measurable increase in median grain diameter through time and more heterogeneous grain size distribution.
From a wider perspective, this research contributes to improve the understanding of the climatic situation that characterised the Younger Dryas in the northern Netherlands.

Table of Contents

1. Introduction

The study focuses on the environmental conditions that characterised the Younger Dryas stage in the Northern Netherlands. For a better appreciation of the topics discussed, the introduction section presents useful information regarding the effects of the Younger Dryas, the aeolian mechanisms and the importance of pingo remnants for paleoclimate researchers.

1.1 The Younger Dryas

The Younger Dryas (YD) is a geological period defined by sharp fluctuations of the global climate, with abnormally cold temperatures in the Northern Hemisphere (Cheng et al., 2020). The YD represents the last stadial of the Weichselian Glacial at the end of the Pleistocene and for this reason, its abrupt ending approximately 11.720 calendar years BP, signals the beginning of the warmer Holocene epoch which extends to present day (Rasmussen et al., 2006) (Walker et al., 2009). The trigger behind this swift change in the global climate is not yet identified with complete certainty, but three main suspects have been investigated in the past. The mega-flood caused by the outflow of freshwater from paleolake Agassiz in North America is the most accepted culprit responsible for initiating the Younger Dryas. This event reduced the sea salinity gradient which drives the Atlantic Meridional Ocean Circulation, limiting the flux of warmer sea water to the coasts of North America and Europe (Murton et al., 2010). Volcanism linked with the Laacher See eruption of 13 ka BP was initially suspected, but the event took place almost 2 centuries before the YD onset, so this theory has also lost credibility (Abbott et al., 2021). The controversial Younger Dryas Impact Hypothesis proposed that a dark layer of charcoal and carbon spherules was the consequence of a celestial impact that caused the Younger Dryas. (Firestone et al., 2007) The theory has lost credibility due to the biased misinterpretation of traces originated from wildfires and volcanism (Leshyk, 2018) (Holliday et al., 2023)(Broecker et al., 2010).
The onset of the Younger Dryas halted the slow warming trend of the global climate that characterised the Weichselian Late Glacial. The most affected area was Greenland which experienced a drop in mean winter temperatures of 9 to 14°C (Buizert et al., 2014).

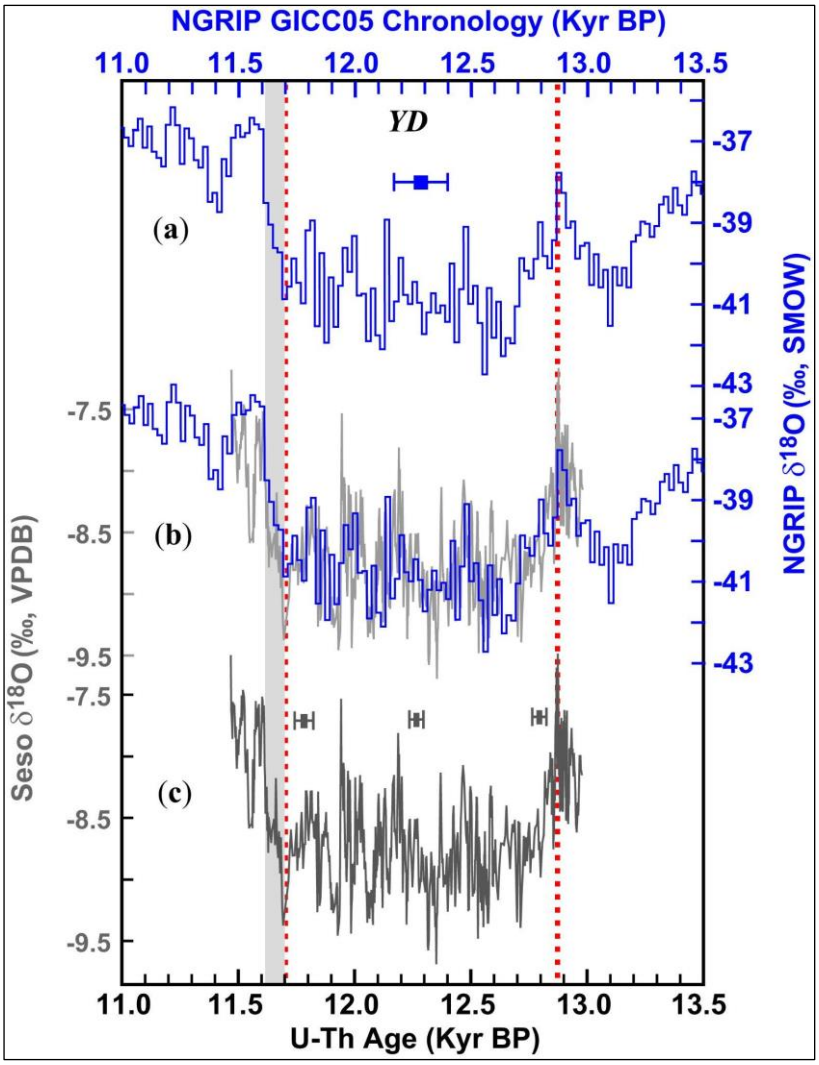

Figure 2. The Greenland ice-core NGRIP data (a) shown in comparison with the Seso speleothem oxygen isotope ratio data (c) with their overlap shown in (b). The red lines indicate the onset and the ending of the Younger Dryas stage while the error bars refer to the error on the age axis (Cheng et al., 2020).

1.2 Aeolian Activity in the Dutch Landscape

The landscape during the Younger Dryas had a very dissimilar appearance to what we are familiar with, characterised by a quite different soil cover, vegetation and climate.
In the Netherlands, the onset of the Younger Dryas has been correlated with the abrupt decline in the pollen count of *Pinus sylvestris*. This stark change is attributed to the reduction of the mean duration of the summer months. Such onset coincided with a distinct cooling of the climate, with mean summer temperatures falling by about 5 °C and winter ones by as much as 13°C (Bazelmans et al., 2021). Previous research suggests that the increase in aeolian activity across the Netherlands was a characterising element of this stage. Key factors are the disappearance of pine woodland, which was substituted by sparser shrubs and grasslands (Hoek, 1997). Vegetational changes of this type allow the seasonal winds to transport a higher amount of sand deposits. Simultaneously, the amount of plant biomass growing and decaying was in decline due to reduced mean annual temperatures (Bazelmans et al., 2021). These two factors together lead to a substantial downfall of the organic content available.

Across this time, the Netherlands lost substantial woodland cover and the fluvial processes experienced a reversal back to periglacial conditions. In the rivers Rhine and Meuse, a shift occurred, identified by an increment in the fluvial discharge causing their predominantly meandered systems to revert to braided channels (Kasse et al., 2020). The Younger Dryas is also characterised by the decline in overall lake levels during particularly the latter part of YD (see fig. 5 in Hoek & Bohncke, 2002). This is thought to have caused a lowering of the water table, leading to more soil aridity and vulnerability to aeolian erosion. (Hoek and Bohncke, 2002).

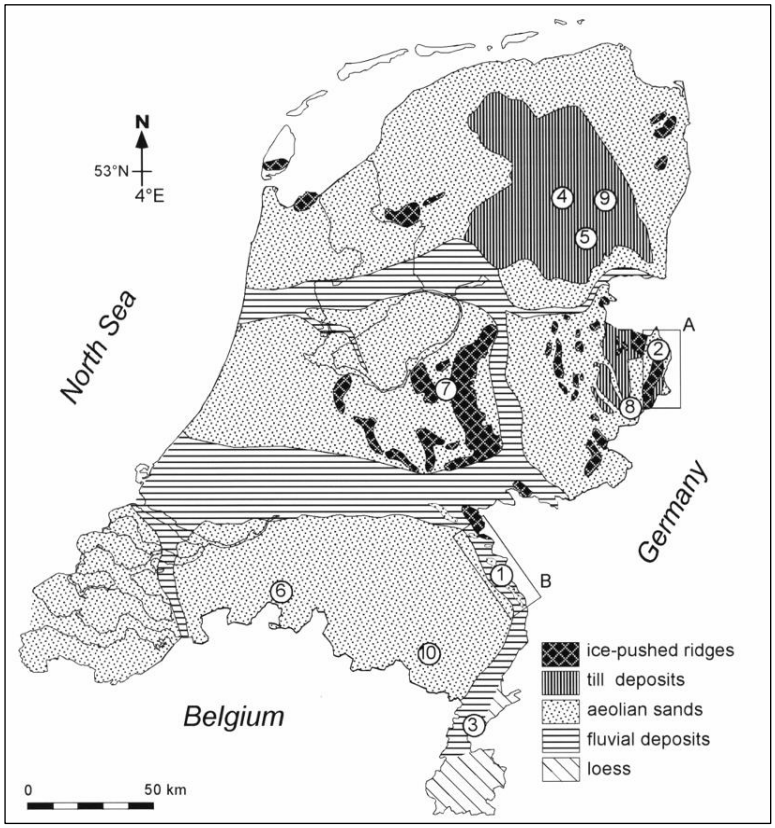

Figure 3. Reconstructed geological landscape of the Netherlands during the Weichselian Late glacial 14.500 - 11.720 YBP (Hoek and Bohncke, 2002).

Climatic fluctuations are the drivers of wide-scale geomorphological shifts such as the biotic and fluvial changes previously introduced. These two elements play a role in the availability and geographical distribution of sources of aeolian sediments. In the litho-stratigraphy, the Younger Dryas is easily identifiable as the layers of Younger Coversand II that forms the uppermost layers of the Boxtel Formation (600 - 11.7 ky BP). This coversand is found between the older Usselo soil and subsequent Holocene soil (www.dinoloket.nl).
From a climatic point of view, the intensification of seasonal south-westerly summer winds and extreme storm events are factors that are believed to have enhanced the sedimentation rate of sand across the Northern Netherlands. (Kasse et al., 2020).
A consequence from such climatic trends is the formation of aeolian river dunes near fluvial channels during the latter half of the YD, the sporadic return of discontinuous permafrost, and the reversal back to predominantly herbaceous cover (Bazelmans et al., 2021). The formation of sand dunes in proximity of major fluvial channels helped researchers to reconstruct the prevalent wind directions of the summer months through the analysis of adhesion ripple cross-laminated profiles (Kasse et al., 2020). The second half of the Younger Dryas is characterised by stronger winds, more common storm events, a decline in vegetation cover and an increase in

aeolian deposition detected across the stratigraphic record. (Hoek and Bohncke, 2002) (Bazelmans et al., 2021) (Kasse et al., 2020).

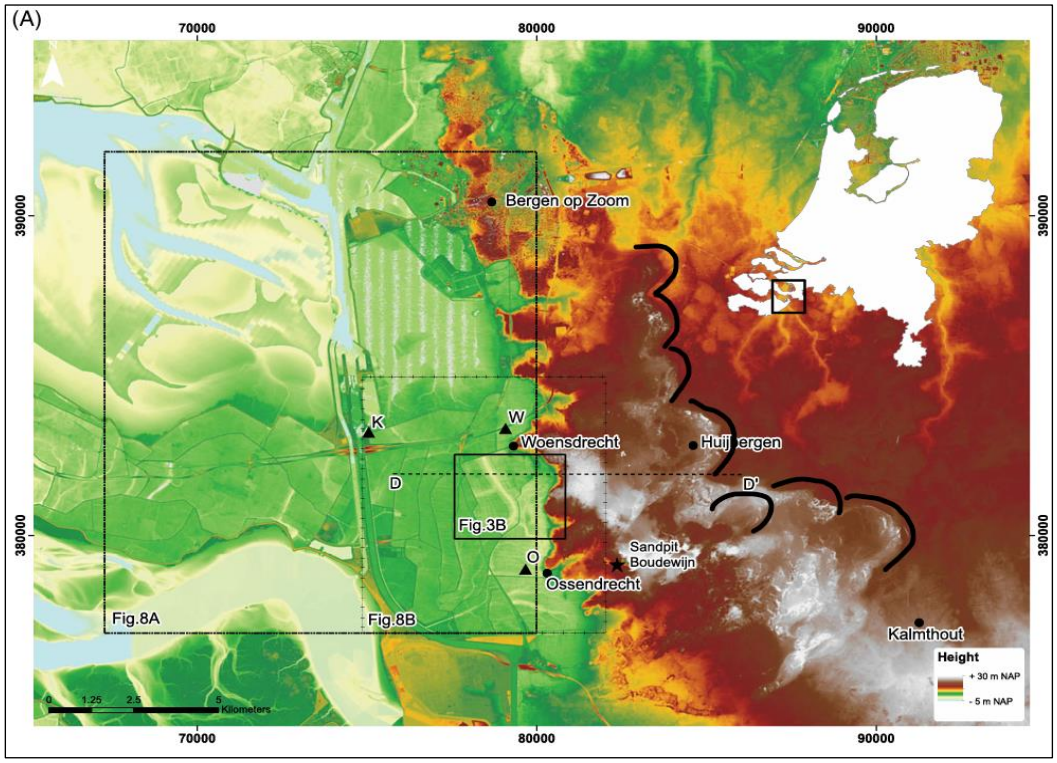

Figure 4. Relief map of the Younger Dryas parabolic dune field found in Brabantse Wal, Zeeland, Southern Netherlands (Kasse et al., 2020).

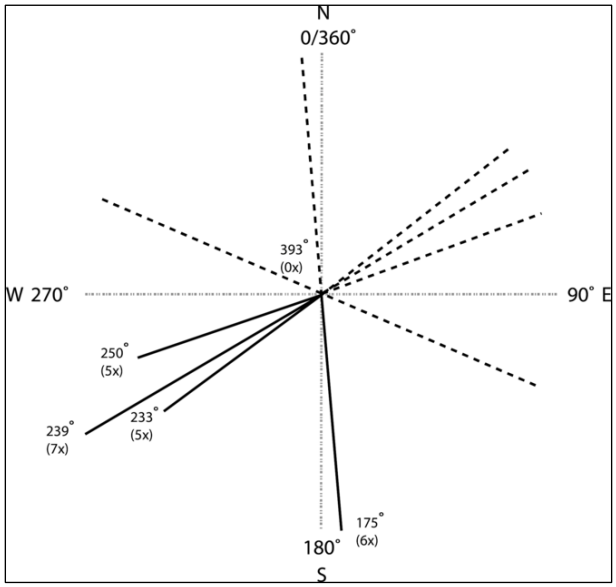

Figure 5. Directional representation of the prevalent winds across the Netherlands during the Younger Dryas stadial based on the observation of ripple sets from 5 lacquer peels (Kasse et al., 2020).

Figure 5 presents the cardinal directions that the ripple sets have been observed to face from the study of Kasse et al. in 2020 and the dominant direction appears to travel from south-west to north-east with the most common headings pointing from 239°, 233°, 250° and an outlier case from south to north heading specifically from 175°.

1.3 Pingo Remnants

Pingos are dome shaped periglacial landforms with diameters ranging from tens of metres up to a full kilometre. They form under a very narrow set of cold environmental conditions and their main identifying feature consists in a lens-shaped layer of permafrost buried beneath a shield of topsoil. Pingo remnants have an ideal morphology for capturing aeolian sediments, which makes them exceptionally useful for researchers that desire to access well-preserved deposits of aeolian sand. For this particular reason, Dutch pinto remnant sites are in the main focus of this study.

Depending on the type of permafrost conditions, pingo remnants are categorised under two groups:
The first category of pingos are called “open-system” or “artesian” and remnants of those are found scattered in the Northern Netherlands (Kluiving, Verbers and Thijs, 2010) (Pidwirny, 2006). This kind of pingo occurs with the presence of discontinuous permafrost and a supply of unfrozen groundwater from beneath. When the artesian pressure from below is directed vertically through permafrost gaps, the topsoil is deformed into a dome shape and a pingo is born. Subsequently, the trapped groundwater freezes and gradually develops an ice lens that keeps growing, in such pingos, their depth is directly influenced by the thickness of the permafrost.

In other cold regions of the world like Canada is found a second type of pingo called “closed-system” which emerges in conditions of continuous permafrost. The growth of this pingo occurs due to water freezing and expanding between an upper layer of frozen infill sediment and an impermeable continuous permafrost layer underneath it. In such cases the initial growth of the ice lens happens in the width dimension and later builds height, sometimes even forming a sub pingo when the hydrostatic pressure is sufficient to lift the main one. The nature of this pingo causes the dome shape to rupture, outflow, fault and change in height with seasonality, as the pressure of the water inside fluctuates (Mackay, 2011) (Mackay, 2002) (Yoshikawa, 2013).

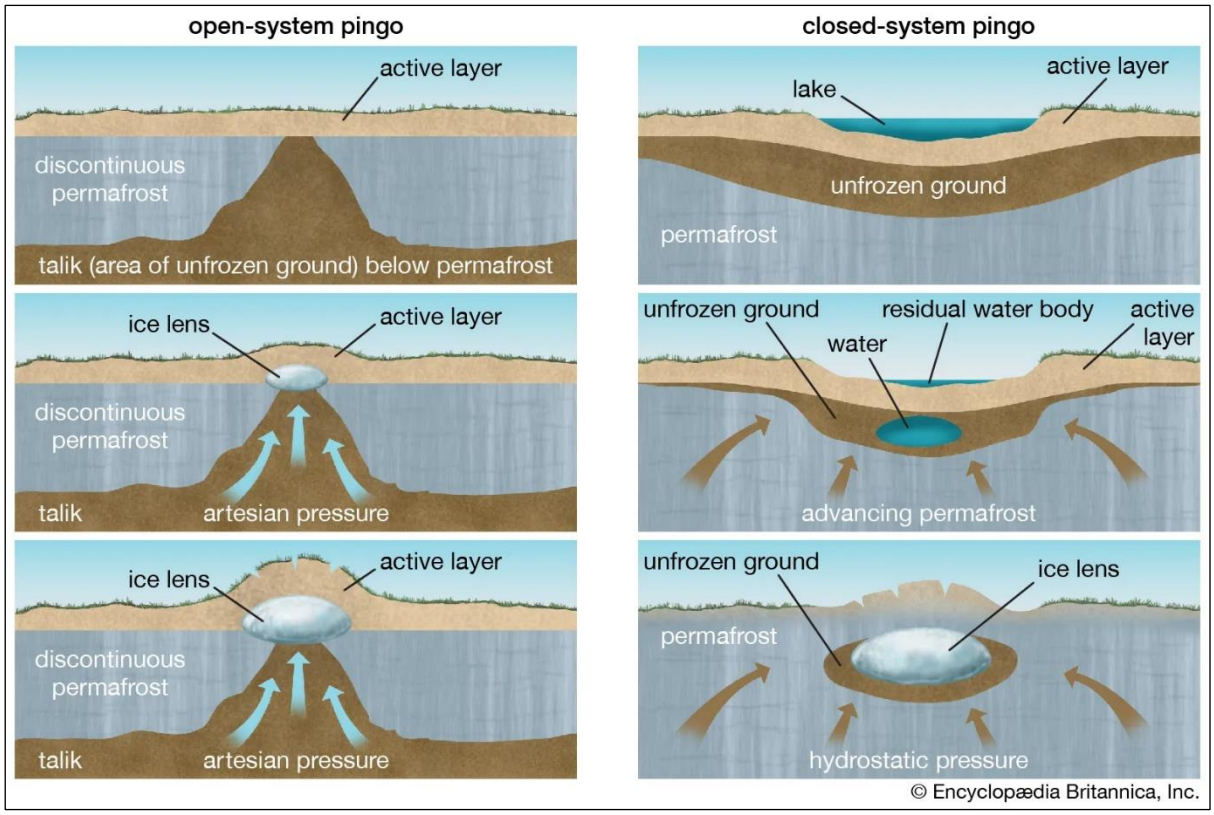

Figure 6. Comparative diagram between the growth of an open-system or artesian pingo (left column) typical of the Netherlands, versus the formation process of a closed-system or hydrostatic pingo common in Canada (Péwé, 2024).

After an ice-age period, pingos experience a physical collapse due to the melting of their permafrost core which can transform them into a crater-shaped lake. In the present day, some collapsed pingo lakes still exist although most have been entirely filled by sediments.

A regional study of the Northern Netherlands discusses two main types of sediments found in the collapsed pingo structures which depend on the topography of the landscape they are found in (Kluiving, Verbers and Thijs, 2010). This latter characteristic is observable easily in height maps of the Netherlands such as AHN Viewer and offers more contextual information about a particular pingo site. In most cases where peat was the main component of the pingo filling, the site was found in lowlands between relatively elevated deposits of glacial till. On the other hand, the study revealed that pingos containing an even fraction of loam and peat were often situated on the most elevated areas of the glacial ridges. The outcome indicates that at lower altitudes it is more likely for a pingo lake remnant to contain a higher-level organic matter which contributes to the formation of a peat bog. In contrast, it was observed that higher pingo remnant sites tend to capture a more balanced mix of organic matter and inorganic sediments likely transported there from aeolian processes. (Kluiving, Verbers and Thijs, 2010). In this study, the four pingo remnants investigated are situated on terrain surfaces characterised by periglacial deposits of the Boxtel, Drenthe and Drachten formations from the Weichselian and Saalian glaciations (www.dinoloket.nl).

The generally undisturbed nature of the pingo fillings found in the Northern Netherlands offers the perfect conditions for the accumulation of sediments dating back in the time of the Younger

Dryas stadial. Sand, silt, clay, pollen and organic matter accumulated throughout the millennia inside the pingo remnants, and they can be studied to gather knowledge of the past climatic and environmental conditions. For this reason, samples from pingo remnant fills are highly valuable because they contain proxies for reconstructing past changes in vegetation cover, air temperatures, wind intensity, fluvial processes, anthropogenic activity in the near surroundings and even volcanism.

1.4 Coring Pingo Remnants

Extracting useful geological data is a process that requires an understanding of the shape, size and depth of the filling of a pingo remnant. Several boreholes are usually extracted in planned straight lines to help plot the initial transects. When no boreholes have ever been extracted from a presumed pingo remnant, it is ideal to take notice of the position of the circular depression shown on an elevation map as the first step. When the position of the pingo is established with precision, the linear transects of boreholes are spatially planned to cross each other at the centre of the pingo. Such arrangement grants the best chance of extracting samples that can be used to generate the most representative cross sections of the pingo filling. This type of graph, an example being figure 8 below, is particularly useful for subsequent studies that focus on the same pingo. The data already collected from previous coring work allows us to understand crucial factors such as maximum sediment depth, peat layers, loam layers and the interpolated profile shape of the layers as shown in figure 8.

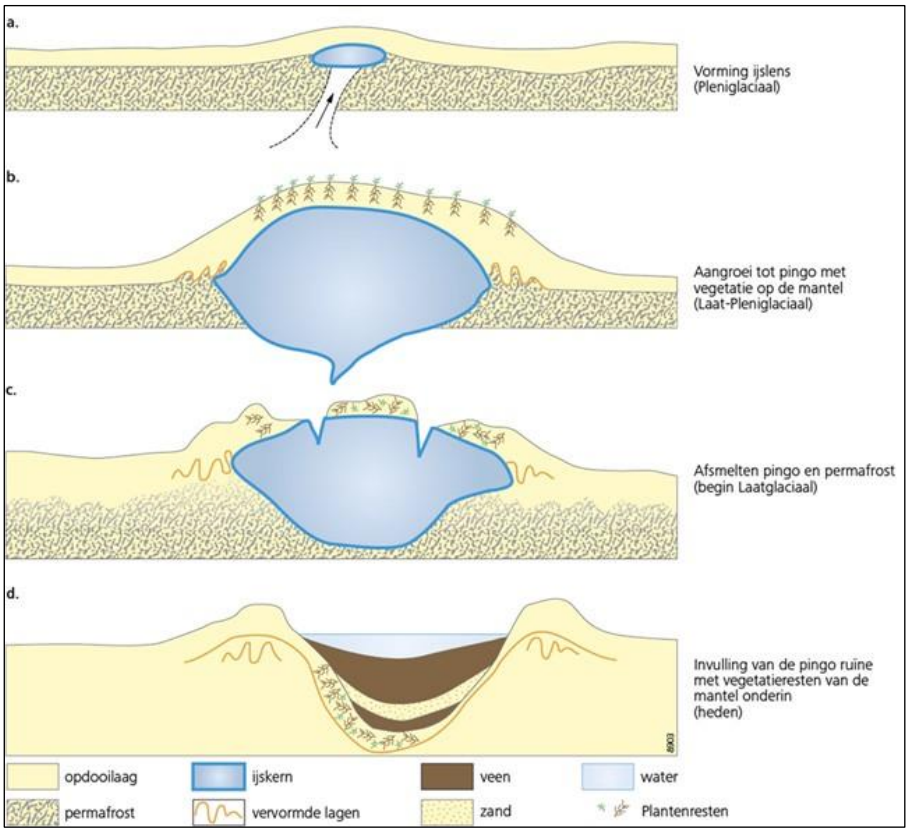

Figure 7. Formation process of an open-system pingo lens under permafrost conditions during the pleniglacial stage of the Weichselian (a), followed by the growth of the pingo during the late pleniglacial stage (b). Subsequently the topsoil fragments and the exposed permafrost starts to melt during the early lateglacial (c). The

structural collapse of the ice lens forms a lake where the cover material causes an almost complete infill of late glacial-Holocene sediments (Stouthamer et al., 2023).

As Fig. 7 illustrates, the open-system pingos like those found in the Dutch region of Drenthe were beginning to melt by the start of the Bølling-Allerød interstadial (GI-1) which preceded the Younger Dryas itself. By the time of the onset of the YD, most pingos had already completely collapsed and transformed into lakes which began collecting aeolian sediments.

The pingo fill shown in the transect of Figure 8, is an example located in the Northern Netherlands, near the town of Veenklooster. This site is one of the four investigated in this study and is shown in chapter 2.2 at page 14, figure 9, where it is displayed as site “D” on the map. Figure 8 shows that in the Veenklooster pingo remnant there is a layer of humic loam at the depths of 2-3 metres between two layers of more organic-rich peat (Kluiving, et al., 2010). Due to the lower organic content of the loam, it can be assumed that this represents the colder period of the Younger Dryas. The intensity of the wind also plays a role because it “filters” the maximum grain size that can be transported from the source into the filling of a pingo remnant.

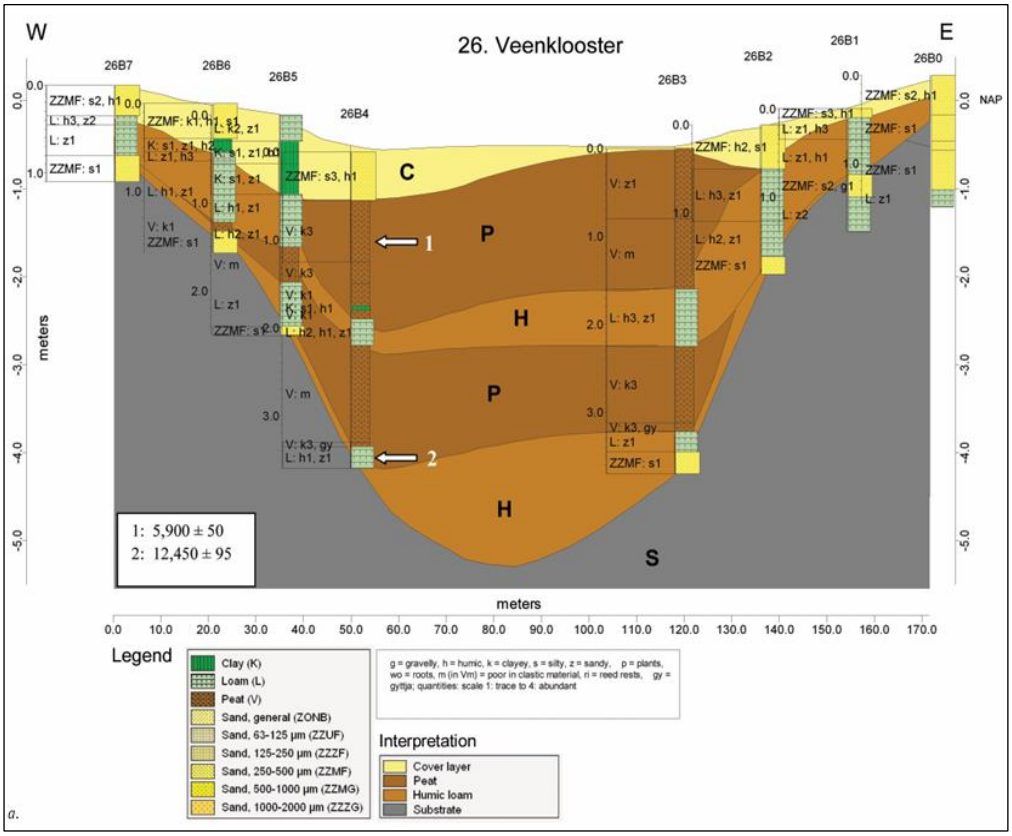

Figure 8. West to East cross section of the Veenklooster pingo remnant, with colours indicating distinct types of material that make up the filling (Kluiving, et al., 2010).

Figure 8 visualises the natural variations between darker, organic, peat-rich layers and generally thinner, lighter and sandier layers of humic loam.
The interpolated convex shape of such sediment profiles between boreholes 26B4 and 26B3 is likely modelled incorrectly, due to the concave nature of the substrate which affects the shape of the layers depositing on top of it.

1.5 Research Question:

The main research question of this study is:

"How sandy was the Northern Netherlands during the Younger Dryas when compared to the previous (Bølling–Allerød) and subsequent (Greenlandian) stadials?"

To answer this question, the topic is broken down into three sub-questions:

1) ***To what extent does the inorganic fraction of sediments increase in pingo remnants during the Younger Dryas period?***

This question dives into the measurement and interpretation of the Loss on Ignition laboratory work conducted on the sediment samples. The objective of this section is to calculate the percentage mass of the sediments composed of inorganic material such as sand and silt. The expectation is to find that the residual mass after the Loss on Ignition increased during the Younger Dryas period when compared to the previous and subsequent chronology due to a multitude of environmental factors.

2) ***Can aeolian activity, as a climatic factor, explain the increase in Younger Dryas sand deposition found in Dutch pingo remnants?***

To explain the aeolian processes acting as the main driver behind the increased presence of sand in the stratigraphy of the Netherlands during the Younger Dryas, the spatial distribution of the soil types at the end of the Boxtel formation is considered. In fact, such formation begins at the Middle Pleistocene and ends with the Holocene (www.dinoloket.nl). With the online service of the DINOloket website, an extensive database of the Dutch substratum can be accessed to analyse the distribution of the sands surrounding the 4 borehole sites of this study (www.dinoloket.nl). According to a previous study focused on the winds characterising the climate of the Younger Dryas, it is possible to know the direction of aeolian sand transportation. This piece of knowledge makes it possible to extrapolate whether the sands discovered in the four pingo remnants is plausibly of aeolian origins (Kasse et al., 2020). Key factors in this work of comparison are the characteristics of the sand deposits neighbouring our 4 borehole sites of study.

3) ***What changes occur in the homogeneity and grain size of the inorganic sediments across the duration of the Younger Dryas?***

Microscope photography is employed to observe in detail the characteristics of the sand and silt components of the four pingo remnant core sites. This tool allows to gather information about the homogeneity of the distribution of sands and silts according to determined categories based on the criteria of grain diameter classes ranging from smallest to largest.
The homogeneity of the grains and their diameter are visually compared between sites or within the same core along its temporal progression to establish connections with fluctuations in the LOI, median sand grain diameter and YD climate.

2. Methods

This portion of the study is subdivided into a series of sections which describe the decision-process regarding the selection of the sites to be investigated followed by the coring methods, field sampling, lab sampling, lab treatments, residual fractionation and measurement of the results.

2.1 Selection of the Coring Sites

Four different collapsed pingo remnants have been chosen for this investigation, their locations are shown in Fig.9 and their names are “Syb” (A), “Ei Van Onnen” (B), “Fraeylemaborg” (C) and “Veenklooster” (D).
As for the first site, the core studied was extracted with the Bohncke-Boor Corer with the first thesis supervisor Dr. Wim Z. Hoek, for the other three sites, the cores had already been extracted and stored in the Earth Simulation Laboratory of the Utrecht Science Park, Netherlands.

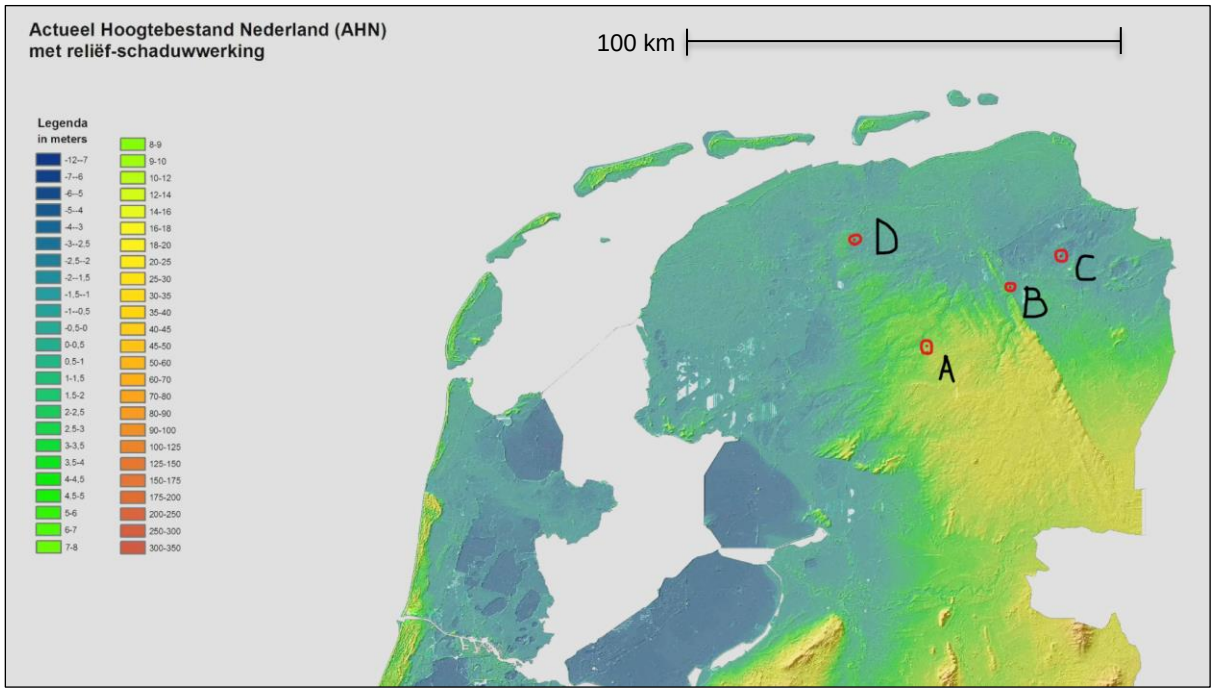

Figure 9. Lidar topographical map of the Northern Netherlands, the four locations of the sites of study are shown. The letters refer to coring sites Syb (A), Ei Van Onnen (B), Fraeylemaborg (C) and Veenklooster (D) (AHN Viewer, 2024).

As shown in Figure 9, the 3 pingo remnants at the sites of Syb (A), Ei Van Onnen (B) and Fraeylemaborg (C) are all located approximately on a shared imaginary straight line that goes from South-West to North-East.

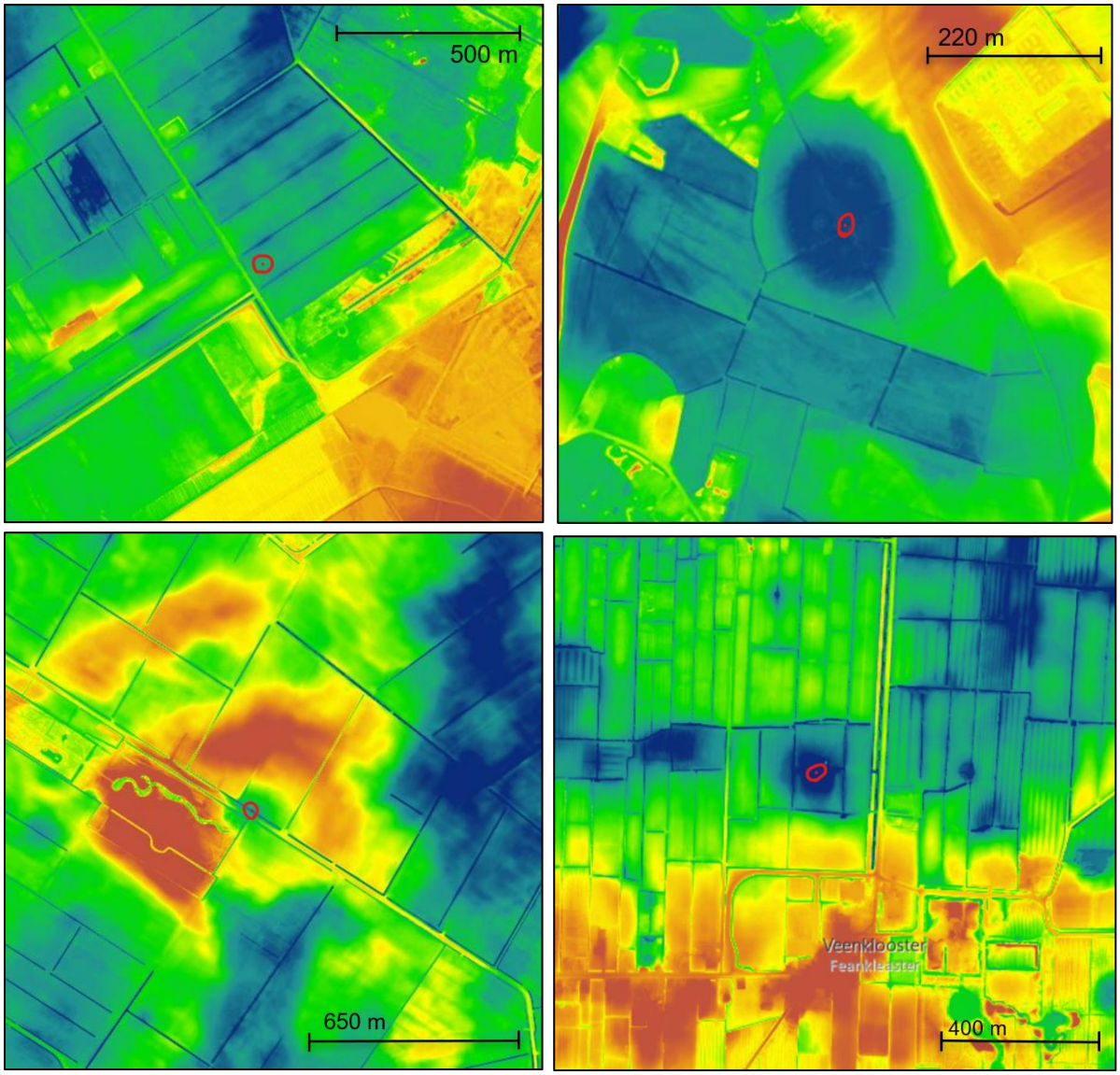

Figure 10 (top-left) shows the local landscape elevation near the Syb site (A), Figure 11 (top-right) shows the local landscape elevation near the Ei van Onnen site (B), Figure 12 (bottom-left) shows the local landscape elevation near the Fraeylemaborg site (C), Figure 13 (bottom-right) shows the local landscape elevation near the Veenklooster site (D) (AHN Viewer, 2024).

All 4 sites share a substrate of similar geological origin because they are characterised by till deposits from either the Weichselian or Saalian glaciations. According to the data shared on the DINOloket database, the Syb site is found above the van Wiedern group of the Boxtel formation (Weichselian glaciation), the EVO site stands above van Gieten group of the Drenthe formation (Saalian glaciation) while the Fraeylemaborg site substrate belongs to both Drenthe van Gieten and Boxtel van Wiedern ground moraines (Saalian) and aeolian sands (Weichselian). The site of Veenklooster, shown on Fig.9 as (D) is found above the substrate originating from the Drachten formation consisting of Saalian periglacial and aeolian sediments.

The decision to study these four particular sites is due to their individual nature and geographical alignment. As collapsed pingos, each of them hosts rich amounts of stratigraphic information of the past environmental conditions. The reason to study them is because 3 out of 4 (A, B and C) are oriented along an imaginary line that travels from South-West to North-East

which aligns with the prevalent seasonal winds of the Younger Dryas (Kasse et al., 2020). This choice allows to gain more insight regarding the aeolian sediments found at three locations because they are approximately aligned along the prevalent wind direction. The idea is to compare the characteristics of the sands found in these three geometrically aligned sites to make observations about the wind and availability of aeolian sediments.

The core extraction took place in the location nicknamed “Syb”, approximately at the geometric centre of the collapsed pingo remnant. This site is near the border of the Province of Drenthe and Friesland, South-West to the Veenhuizen village at the coordinates 53°01'20.5"N 6°22'38.0"E. A cross section was made by Syb de Vries and Peter Vos and the coring location was at the deepest point in the central region of the presumed pingo remnant. The other 3 pingo remnant sites were already cored and extracted prior to the study and their cores were sampled directly at the Earth Simulation Laboratory (ESL) located at the Utrecht Science Park.

The other 3 sites are located at the following coordinates:

- Ei Van Onnen (EVO) = 53°08'52.9"N 6°38'22.3"E
- Fraeylemaborg = 53°12'36.4"N 6°49'48.8"E
- Veenklooster = 53°42'42.8"N 6°6'16.2"E

A helpful tool for detecting pingo remnants based on the soil topography are height maps generated using lidar technology which helps reveal the slightest, sub-metre scale variations in the soil that could indicate the presence of an ancient pingo remnant. AHN-Viewer (figure 9) is a great tool used to access the entirety of the Netherlands in the form of high resolution lidar data (AHN, n.d.). Nationwide geological borehole databases like DINOloket for the Netherlands offer an accessible library consisting of hundreds of thousands of borehole measurements containing useful sedimentological and hydrological data (www.dinoloket.nl, n.d.). Such digital tools are especially useful for extensive meta-analysis studies on large spatial scales.

2.2 Sampling (field)

The first 40 cm of topsoil consisted of ploughed material, a half-open shaped auger corer was operated by a simple handlebar with the objective to initiate the borehole and dig a beginning passage for the subsequent coring tool.

- The main coring procedure was conducted in the field with an adapted Livingstone piston corer (Bohncke-boor). This piston-corer offered the advantage of little contamination for the samples, required at least 3 people to operate and each extraction consisted of approximately 1 metre by 6 cm in diameter.
- To continue coring the same borehole after performing the first soil extraction, the piston core was emptied of the sample and a 1 metre extension rod was added between the corer and the handlebars to increase the operating depth of the overall corer.
- Each metre of extracted core sample was packed in plastic film and PVC liner and labelled with numbers to indicate the presumed depth interval for identification in the lab and storage. For structural support and storage, each core section was stored in PVC pipe sections as enclosures.

- As depth increases, so does the required force to push the corer which required 3 people to coordinate their force on the handlebars. The force required for extracting the core at a greater depth is also higher in demand; to overcome this difficulty, an Archimedes lever and chain was used to increase the torque of extraction.
- Photographs were taken at each step of the Bohncke-boor coring procedure to document the method of extraction, on-field observations and the appearance of freshly cored samples before oxidation altered the colour of the peat layers.

While the only borehole practical work was executed at the “Syb” pingo remnant, for this study, previous sediment samples from the 3 other pingo remnants across the Northern Netherlands were adopted for the laboratory activities.

Between the moment of extraction and laboratory analysis, the objective is to mitigate the effects of oxidation of the organic component of the core samples to preserve it in its original conditions. For indefinite preservation, each core is secured in a closed plastic film which is enclosed inside two halves of a PVC tube that protects the sample from structural deformation. A thick plastic bag is wrapped around the PVC structure and sealed with tape to offer a further layer of air-tight protection. Storage happens in a cold chamber at 4 degrees Celsius.

Figure 14. Photo taken during the coring at the Syb pingo remnant, October 2023 (L. Bonanno and W.Z. Hoek)

The samples were ideally exposed to the air for the least time possible to limit the exposure to oxygen which causes cracks in the core to turn from light brown to darker tones. Another side effect of prolonged exposure was a size reduction of the sample due to humidity loss which also affected the overall mass.

2.3 Subsampling (lab)

The cores are photographed and organised by their depth ranges to understand the extent of the sedimentological coverage that they characterise. Several boreholes were taken in proximity of each other and compared the depths and strata from different cores to identify common depositional layers. When sediments were contaminated or missing for a core, the data from the neighbouring ones was used to fill that gap of knowledge.

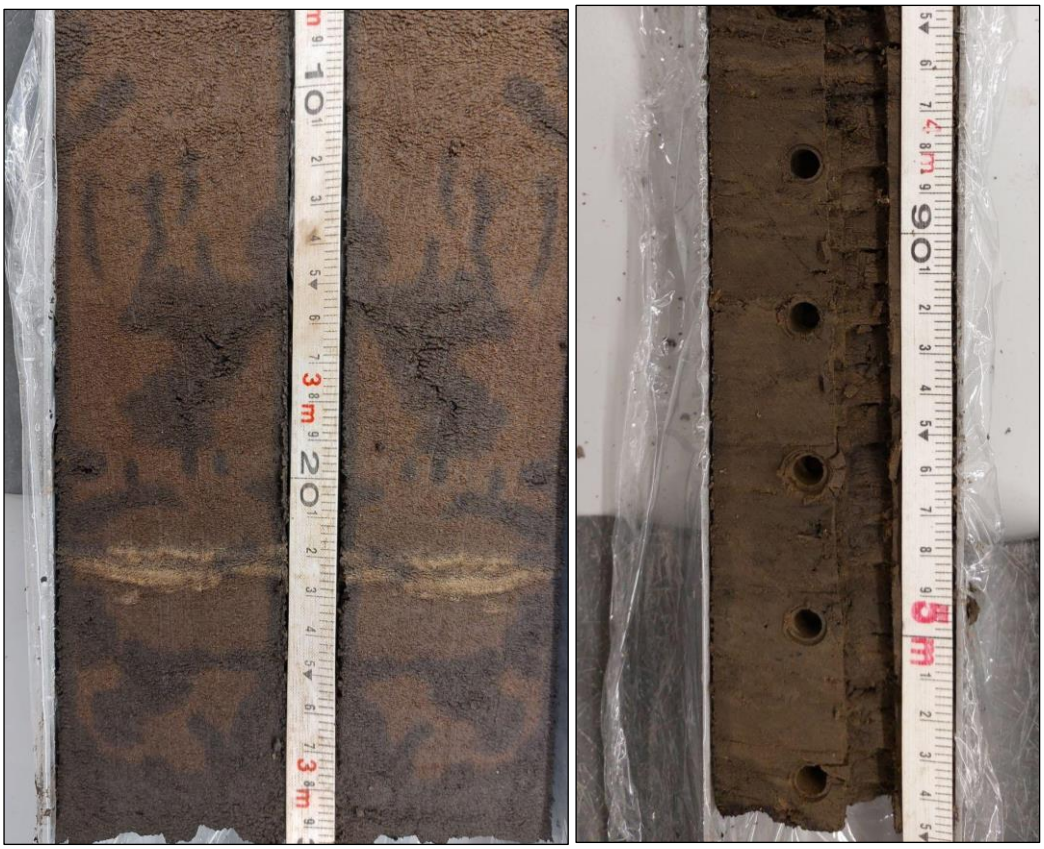

Figure 15. Photographs taken in the lab of the Syb core. A sandy layer is seen at the 322 cm depth which later was sampled (left) while the peaty core of Fraeylemaborg (right) is sampled at regular intervals by Dr. Wim Z. Hoek for palynological analysis (L. Bonanno, 2023).

Each core was photographed with the metre tape parallel to it for identifying the range of sedimentological depth being observed as shown in Figure 15. This helped to organise photographs and plan for selecting the sampling depths of most interest.
The presence of a visible organic-rich peat to silty sand transition was expected based on findings available from other studies and was interpreted as the transition between the Younger Dryas and the early Holocene approximately 11.700 cal. BP.

This step of the study consists of treating the samples extracted from the cores of the 4 pingo remnant sites to generate data and make calculations that provide insights on the paleo-environmental conditions of the Netherlands during the Younger Dryas. The main parameters measured include the percentage mass difference between each sample before and after the LOI treatment, the median grain size for the sand and silt particles after their fractionation and the sand to silt mass ratio for each sample.

2.4 Loss on Ignition

The Loss on Ignition method is employed to determine the proportion of organic matter contained in a fresh dirt sample extracted from a core. This process consists of using a dryer and subsequently an oven to remove the water content and combust the organic matter from the samples. This process aims at removing any other material from the samples that is not inorganic sediment. The determination of the organic content is calculated by subtracting the

mass of the residual mass after the LOI treatment, to the original starting mass of the sample. (Heiri, Lotter and Lemcke, 2001)

Figure 16 shows the darker core samples that have been dried and need to be ashed for LOI. The smaller crucibles contain ashed samples which are significantly inferior in mass and size (L. Bonanno, 2023).

The purpose of the Loss on Ignition step for this project is ensuring that across the stratigraphical depth axis of each core the results for the wet mass (M1), dry mass (M2) and ashed mass (M3) are obtained from each sample. This gives insight on the lithological changes occurring in terms of soil water content and organic vs. inorganic matter composition.

1) At regular 1 cm intervals, 1 cm^3 was cut with a small knife, out of each core sample and the depth was documented in a data table.
2) The cubes of sediment extracted out of the core samples were stored in ceramic crucibles of which their empty masses had been measured on a high precision balance.
3) The crucibles were kept in a known and identical order of arrangement along their tray to keep track of which samples they each contained.
4) The masses of the crucibles with their cubes of sediment were measured on the high precision balance and recorded. This step ideally should take as little time as possible to reduce the effect of mass reduction in the sediments due to their water fraction evaporating into the atmosphere.
5) Each tray containing the crucibles with the sediments was dried for at least 8 hours at 105 degrees Celsius. Following the treatment, each crucible was weighed to determine the water content as a fraction of the initial sample mass.

6) The samples were ashed at 550 degrees Celsius for a minimum of 4 hours and let cool down for several hours. The masses of the crucibles were measured again with the high precision balance to estimate the percentage mass of the sample that was composed of organic versus inorganic material. The inorganic residuals were preserved for further investigation.

Figure 17. A tray of ashed samples in small crucibles are ready to be weight measured and fractionated with the sequence of sieve filters (L. Bonanno).

2.5 Inorganic Sediment Fractionation (Sand & Silt)

The analysis of the grain size, sand-to-silt ratio was conducted on the LOI residuals taken from each of the 4 cores from the 4 pingo remnant sites. The choice for which particular depth to investigate was established based on the interpretation of the Loss on Ignition results and also by direct observation of the cores themselves. For example, when a thin layer with a colouration different to that of the surrounding loam was identified, it was selected for grain size analysis. A layer of sediment with a lighter colour could signify a brief period of increased aeolian sediment deposition. The intent was to find and study the key points in time that translated into slight changes in the LOI throughout the Younger Dryas which could be linked with abrupt climatic shifts.

Sand Fractionation

The process of sieving allows to fractionate the inorganic residuals of the sediments used for the Loss on Ignition phase of the methods to gather further information about the sand and silt components. This phase aims at dividing the inorganic sediments from each of the sieves into separate categories according to the criteria of grain diameter classes. The outcome of sieving is to produce several categories of varying mass representing the different grain sizes of the sand component of the sediments and ultimately to separate the silt component for further study. Sand fractionation and the separation of silt was done by pouring the ashed sediments into a vertical sequence of stacked sieves of decreasing diameter filter passage. Any sediment of diameter inferior to 53µm was collected in the lowermost container and considered silt.

Table 1 shows the diameters that the sieve filters are designed to intercept for the sand particles, they are in a decreasing order arranged in a double logarithmic sequence.

Sieve Filter (µm)
600
450
300
212
150
106
75
53
>53

Instruments used:

- 8 sieves (of different filter ⌀)
- Steel bottom container (for silt residue)
- Vibration platform machine
- High precision digital balance
- Brush (for cleaning sieves and container)
- 1 x ceramic crucible (for each ashed sample)
- 2 x 100 ml steel cups (for sand & silt fractions)

A total of 8 sieves were arranged with the greatest filter diameter (600µm) at the top and the finest sieve filter (53µm) located at the lowest level with a container at the bottom.
The diameters filtered by the sieves were approximately arranged in a double logarithmic scale. With smaller filter diameters, the size gap between adjacent sieves became smaller, according to a double natural logarithmic scale.

Sieving procedure:

1) Each sieve was cleaned with a brush and its mass measured when empty at first.
2) Ashed sample is poured on the uppermost sieve (of widest passage ⌀ of 600 µm).
3) The stack of sieves was placed on top of the vibrating platform machine and screwed firmly from the top.
4) The vibration platform is activated for 10 minutes to shake and fractionate the sediments.
5) Each sieve mass is measured again with the high precision balance.
6) The mass difference for each respective sieve is used to calculate the absolute mass for the sediments captured for each ⌀ interval.

Silt Fractionation

The residual of sediments collected at the bottom of the sieve stack is considered silt due to its diameter being inferior to the 53µm conventional boundary between sand and silts.

This mass of silt sediment is separately stored from its sand counterpart for each of the 1cm^3 ashed samples for further study.
The aim is to fractionate the silt sediments into 8 categories arranged in decreasing grain diameters. The differences between each category are approximately organised on a double logarithmic scale as shown in table 2.

Liquid suspension is the method used to fractionate the silt component of the inorganic sediment samples. This procedure involves the use of glass tubes filled with water mixed with silt sediments. The aim is to extract the liquid from a given depth at a given time after the mixture is left to fractionate based on the variations in density between the water and the silt component. Due to the completely inorganic nature of the sediments fractionated, no mutual cohesion issues were present. No hydrogen peroxide or hydrochloric acid treatment was required. The maximum mass of silt ever used at once with a single tube filled with 1 litre of water was 2.17 grams, a quantity inferior to the 20 g/litre threshold which is a conventional limit to prevent mutual particle collisions from affecting the measurements.

Table 2 shows the diameters filtered through the suspension in liquid method for fractionating the silt component of the LOI residuals.

Silt Grain Size (µm)
37.5
26.5
18.75
13.25
9.037
6.625
4.5185
3.3125

Tools used (per each sample of silt):

- 1 litre glass test tube
- 1 steel cup (with the silt sample)
- 8x 100 ml steel cups (labelled with different silt grain ⌀)
- 20 ml glass pipette
- Glass cover slide (for the tube)
- Digital stopwatch
- Measuring tape
- Non-permanent marker
- Room thermometer
- 500 ml beaker of distilled water (for cleaning the pipette)
- Oven (for drying the samples in the steel cups)

Preparation procedure:

1) Pour 1 litre of distilled water into the glass test tube.
2) Mark with a line the water depth of 10 cm on the tube.

3) Cover the tube with the glass slide and wait for at least 12 hours to let the water temperature match the room temperature.
4) Fill the 500 ml beaker with distilled water.
5) Measure the room temperature with the thermometer.

Sediment suspension can be accurately predicted through its own formula. The objective is to precisely extract out of the 1 litre test tube the silt sediments of specific classes distinguished by grain diameter.

2.6 Calculations

Velocity of Particle Deposition (Stokes Law)
The formula for calculating the sedimentation rate demonstrates that it is possible to extract silt particles out of the test tubes of a particular diameter given that other parameters are known such as the time of sedimentation, water depth, temperature and viscosity (Sir Horace Lamb, 1945).

$$v_p = \frac{(\rho_p - \rho_w)d^2 g}{18\mu}$$

Table 3 shows the parameters (first column), symbols (second column), SI units (third column) and numerical values (fourth column) that play a role in the Stokes Law rearranged for finding the particle velocity of deposition.

Parameter	Symbol	Units	Value
Particle deposition velocity	v_p	m/s	N/A
Particle density	ρ_p	kg/m^3	2650
Fluid density	ρ_w	kg/m^3	997.7
Particle diameter	d	m	N/A
Gravitational acceleration	g	m/s^2	9.81
Liquid dynamic viscosity	μ	$Pa \cdot s$	$9.433 \cdot 10^{-4}$

Time Calculation Example:
Given such a formula, the rate of sedimentation is calculated for silt particles of the various diameters previously shown in the table 2, expressed as V_p.

The known parameters are:

- Particle density (ρ_p) = 2650 kg/m^3
- Fluid density (ρ_w) = 997.7 kg/m^3 @ 22.5 °C
- Particle diameter (d) = [see table 2]
- Gravitational acceleration (g) = 9.81 m/s^2

- Liquid dynamic viscosity (μ) = 9.433*10^-4 $Pa \cdot s$ @ 22.5 °C

$$9.433 \cdot 10^{-4}$$

For the silt grain size of 37.5 µm the particle deposition velocity is:

$$V_p = \frac{(2650 - 997.7) \cdot (3.75 \cdot 10^{-5})^2 \cdot (9.81)}{18 \cdot (9.433 \cdot 10^{-4})} = 1.342 \cdot 10^{-3} \text{ m/s}$$

Thus, it is calculated that at a water depth of -10 cm, the time elapsed for extracting silt particles no greater than 37.5 µm in diameter is:

$$t = \frac{h}{v} = \frac{0.1\ m}{1.342 \cdot 10^{-3}\ m/s} = 74.49\ s$$

A time that can be rounded to 1 minute and 14 seconds.

The same equation is calculated for all the other silt grain sizes from table 2.
The table 4 presents the time (t) required to extract a mixture of silt of diameter equal or inferior to the size shown in the next column.

Table 4 shows the waiting times used for the fractionation of silt (right column) in relation to the maximum diameter of silt particles that is being extracted (left column).

Silt max. diameter (µm)	Waiting time @-10cm and 22.5°C
37.5	1 minute 14 seconds
26.5	2 minutes 29 seconds
18.75	4 minutes 58 seconds
13.25	9 minutes 57 seconds
9.037	21 minutes 23 seconds
6.625	39 minutes 47 seconds
4.5185	85 minutes 31 seconds
3.3125	159 minutes 7 seconds

Silt fractionation procedure:

1) Toss and mix the silt residue from the steel cup into the test tube.
2) Place the tube onto a stable table surface and start the digital stopwatch.
3) At the 8 predetermined times, insert the pipette into the tube, vertically making sure the tip is located at the 10 cm depth mark.
4) Extract 20 ml of tube water into the pipette and pour it into the steel plate labelled with the grain ⌀ assigned with the predetermined time of extraction.
5) Clean the pipette by extracting and pouring out 20 ml of distilled water from the 500 ml beaker.

6) Repeat the above steps for each of the 8 grain diameters linked to the 8 predetermined times, for each of the silt samples.

Silt Fractions Mass Calculation:

1) Dry at 105 °C every steel cup containing the test tube waters for >8 h in the oven.
2) Weigh the mass of each cup containing the dry silt residuals for the 8 diameter categories.
3) Empty all of the dried silt cups back into the original test tube, brush them clean.
4) Weigh the mass of each clean steel cup again with the high precision balance.
5) Calculate the mass changes for the cups to determine the absolute mass for the 8 silt fractions per each initial silt sample.

2.7 Long-Term Sample Storage

The proper storage for the sediments begins by emptying the water content of each test tube to return the silt sediments for each sediment sample in their respective steel cups. The purpose is to keep sand and silt sediments in two separate dedicated steel cups per each of the samples extracted from the pingo remnant cores.

Water is extracted carefully out of the test tubes with the aid of the 20 ml glass pipette, with attention to avoid turbulence in the tubes which would suspend the silts found at the bottom. When >100 ml of silt and water are remaining in the bottom of the test tube, the contents are poured into a single steel cup designated for the storage of the whole silt fraction for each sample of sediment. Each of these silt cups are dried in the oven at 105 °C for >8 hours.
As a precautionary measure, the mass of the silt cups with the silt contents is measured after all the above steps are completed to help calculate the amount of silt mass lost due to the various transfers happening throughout the liquid suspension fractionation.
Once the final masses for sand and silts are recorded per sample of sediment per each core, the contents can be stored in a dry and protected environment.

2.8 Sediment Microscopy

To further investigate the visual aspects for the sand and silt grains of the sediments, microscope photography is employed.
Conventional microscope glass slides are prepared for storing exceedingly small amounts of sand or silt that can be observed under an optical microscope equipped with a digital camera.

Preparation Tools:

- Glass microscope slides
- 0.2 mm thick glass coverslips
- Glycerin (adhesive for the sediments)
- Small precision metal tweezers
- Small precision blade
- Small measuring spoon
- Electric heater platform
- Fine-tip permanent marker

Preparation Steps:

1) Scratch a small amount of sand / silt out of the steel cup with the measuring spoon.
2) Place the sediment on top of the microscope slide.
3) Cut a cube of glycerin (approximately 3 x 3 mm) with the blade, position it above the sediment on the slide.
4) Heat the slide on the heater platform (70 - 140 °C) for 1-2 minutes to melt the glycerin.
5) Position the glass coverslip on top of the glycerin + sediment mixture, let it cool down and solidify.
6) Label with the marker the microscope slide. Indicate core name, depth (cm) & type of sediment (sand or silt).

Microscope slides are photographed through an optical microscope, with an integrated digital camera apparatus at a 400x magnification. The individual images are stitched together automatically to construct higher-resolution photo-mosaics. The observation of the pictures helps to interpret the individual features of the sand grains and glance at the collective heterogeneity of the diameter and shape of the particles.

3. Results

3.1 Sand Distribution by Grain Size

The way in which the distribution of sand grain size categories of a sediment sample is represented is using a colour coded pie chart. The categories have been calculated with the sand sieving fractionation method explained earlier. The range of each category diminishes in scope in a double logarithmic manner when compared to its neighbouring categories.

To each grain size interval, a colour has been assigned to:

Table 5 shows in the left column the sand grain diameter in categories, linked with their respective pie chart colour in the central column. The respective sand category names are presented in the right column.

>600 µm ⌀		Very coarse sand
600-425 µm ⌀		Coarse sand
425-300 µm ⌀		Coarse to medium sand
300-212 µm ⌀		Medium sand
212-150 µm ⌀		Fine sand
150-106 µm ⌀		Very fine sand
106-75µm ⌀		Extremely fine sand
75-53 µm ⌀		Extremely fine sand

The complete library of all the pie charts for all of the samples produced in this research is available in the appendix section.

3.1.1 Syb Median Grain Size Trends

Figure 18 shows grain size categories by relative percentage mass at a given core depth of 418-419 cm at the Syb pingo remnant site which is the deepest and oldest of the 10 samples taken. The relative masses for the sand categories between 425 and 75 µm are in relatively similar proportions ranging between 7 - 15% and a very small mass is measured of sands coarser than 425 µm. The greatest sand fraction consists of the finer half of the extremely fine sand (blue), however, the median grain size falls approximately in the median point (90.5 µm) of the coarser half (106-75 µm) of the extremely fine sand in dark green. This sample demonstrates that the fine and extremely fine sands dominate the mass composition of the inorganic residue of the sediment at 418-419 cm of depth in the Syb pingo remnant. The 2% in purple occurs due to the presence of only a handful of very coarse sand particles.

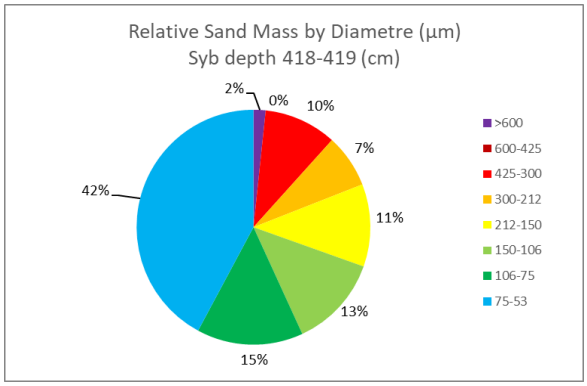

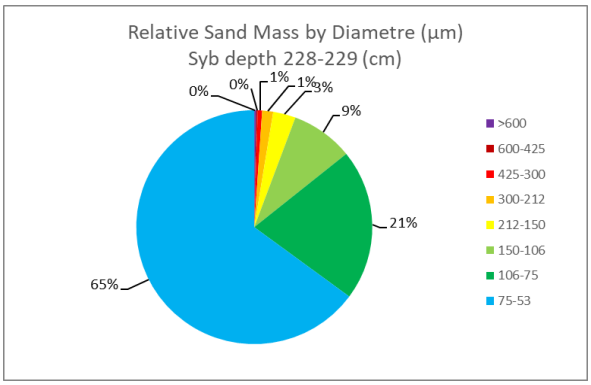

Figures 18 (left) and 19 (right) represent the relative sand mass fractions of the loss on ignition residuals from the sediments found in the Syb pingo core at depths of 418-419 cm (left) and 228-229 cm (right).

Figure 19 demonstrates the different distribution of the sand particles found in the shallowest (228-229 cm) depth of the Younger Dryas coversand layers from the same core as the previous sample. The sum of all sand categories ranging from very coarse to fine sand (purple to bright yellow) barely adds up to 5% of the overall mass, leaving the majority of the mass to the three finest categories. This situation presents a less equally distributed mass across diameter classes, with a more homogeneous composition dominated by very fine to extremely fine sands that take 95% of the overall sample mass. In this scenario the median grain size falls into the coarser half of the blue category, unlike what has been found in the previous, more evenly distributed sample. The interpretation of such distinctive changes in the sand composition is explored in the discussion of the research paper.

3.1.2 Ei Van Onnen Median Grain Size Trends

Figure 20 shows grain size categories by relative percentage mass at a given core depth of 447-448 cm at the Ei Van Onnen pingo remnant site; this sample is the deepest and oldest of the 9 samples studied for this core. The finer half of the extremely fine sands is about one third of the entire sample mass and the largest single category, however, the median grain size falls approximately in the median point (90.5 µm) of the coarser half (106-75 µm) of the extremely fine sand in dark green. This sample demonstrates that the fine and extremely fine sands dominate the mass composition of the inorganic residue of the sediment at 447-448 cm of depth. Almost one quarter of the mass is composed of very fine sand followed by only 10% of fine sand and sands coarser than 212 µm consist of only 3% of the mass.

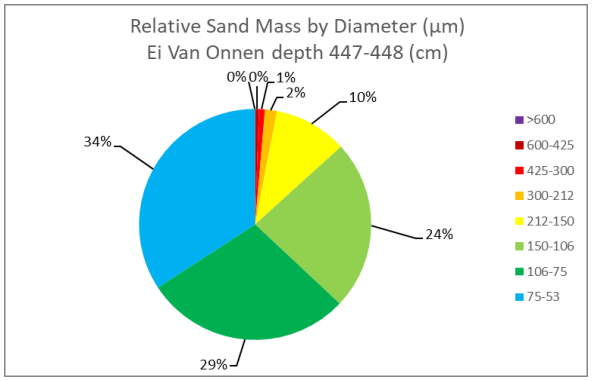

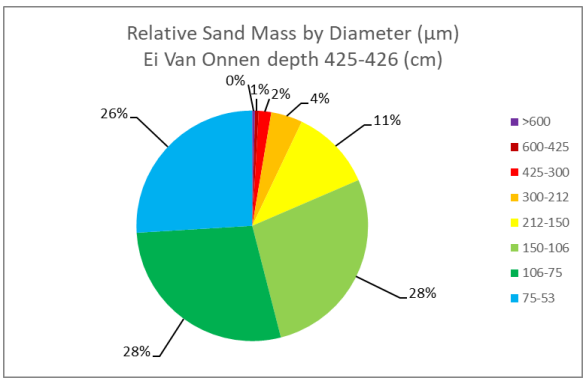

Figures 20 (left) and 21 (right) represent the relative sand mass fractions of the loss on ignition residuals from the sediments found in the Ei Van Onnen pingo core at depths of 447-448 cm (left) and 425-426 cm (right).

Figure 21 demonstrates the different distribution of the sand particles found in the shallowest (425-426 cm) depth of the Younger Dryas. The sum of the extremely fine sands (blue and dark green) covers more than half of the entire sample weight. The medium and fine sands (yellow and orange) barely constitute 15% of the remaining mass, with anything coarser having a negligible impact on the overall mass of the sediments.

3.1.3 Fraeylemaborg

Figure 22 shows grain size categories by relative percentage mass at a given core depth of 496-497 cm at the Fraeylemaborg pingo remnant core. This sample was taken at the deepest point of all the 5 samples taken in Fraeylemaborg. The finer half of the extremely fine sands is the single greatest category by mass of the entire sample; however, the median grain size is found within the coarser half (106-75 µm) of the extremely fine sand.
In this sample, the three finest sand categories (blue, dark green, bright green) occupy more than 80% of the overall sediment mass. Differently to previous cases, the masses of the medium and coarse sands achieve similar levels this time between 4 - 7% each and the very coarse sand (>600 µm) is absent.

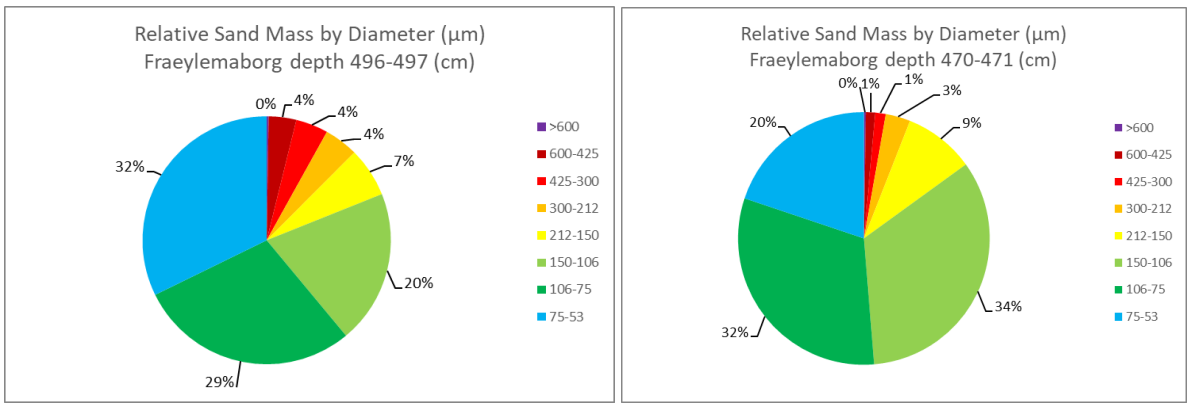

Figures 22 (left) and 23 (right) represent the relative sand mass fractions of the loss on ignition residuals from the sediments found in the Fraeylemaborg pingo core at depths of 496-497 cm (left) and 470-471 cm (right).

Figure 23 breaks the previously established norm by having the fine sand fraction being the largest at 34% closely followed by the coarser half of the extremely fine sand at 32% and the finer slice of the extremely fine sands (blue) only taking 20% of the general mass. This drastic change demonstrates a general coarsening of the sand across the spectrum, though the median size remains constrained to the same diameter category as the other sample taken in the Fraeylemaborg core. What the median grain diameter category fails to highlight, is that this time the true median is much closer to the 106 µm limit that divides the extremely fine sands with the fine ones. For this reason, pie charts offer the best overview of the grain distribution.

3.1.4 Veenklooster

The pie charts present the grain size fractions by relative percentage mass at the respective depths of 200-201 cm (left) and 180-181 cm (right) of the Veenklooster pingo remnant core. In the deeper sample (figure 20), the major category is the finest half of the extremely fine sand at 42% with the subsequent coarser ones of progressively inferior value, despite this, the median value falls on the second finest fraction in proximity to its internal median diameter of 90.5 µm. Unlike in other samples, here the sand content is detected throughout all the grain size categories and with the very coarse sand contributing for 2% of the overall mass.

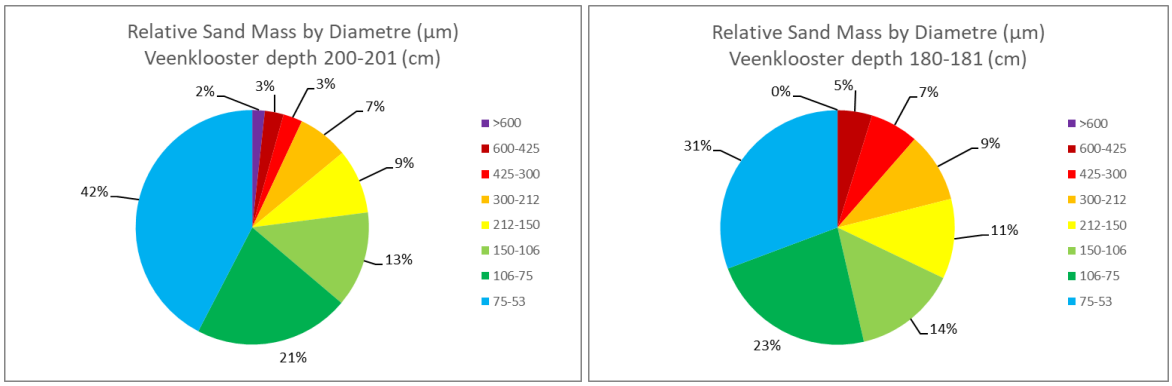

Figures 24 (left) and 25 (right) represent the relative sand mass fractions of the loss on ignition residuals from the sediments found in the Fraeylemaborg pingo core at depths of 200-201 cm (left) and 180-181 cm (right).

The shallower sample on the right (figure 25) presents a similar scenario at a first glance, however there are subtle differences throughout. The finest sand category (blue) this time is 11% inferior in mass when compared to the deeper sample in figure 20. The median value is still located in the coarser half of the extremely fine sands which as a category is very similar in size as its counterpart from the deeper sample. The mass for the three categories within 106 - 300 µm remains again similar to those found on the deeper sample, however his time the masses of the two coarse sand categories (shown in shades of red) take up a larger portion of the mass. No trace is detected of the very coarse particles at <600µm.
Further interpretation of the data is located in the discussion section of this report.

3.2 Sand/Silt Ratio

The sand to silt mass ratio is an index that aims at measuring the proportional disparity of the inorganic sediments in a sample that fall into 2 categories: sand for grains > than 53 µm versus silt for grains in diameter < than 53 µm. The evolution of the sand/silt ratio throughout the Younger Dryas in a core from a pingo remnant can indicate that changes in the aeolian sediment characteristics did occur. Such variations could be linked to fluctuations in the intensity of aeolian activity or in changes of the availability of neighbouring aeolian sediments.

3.2.1 Syb

The changes between the portion of silt ad sand in the form of the, distinctly fluctuates throughout the Younger Dryas. The tendency of this ratio to include a higher proportional content of sand as time progresses is in direct contrast with the other trend seen where the median sand grain size tends to diminish over time. While the sand median grain size decreases, the silt presence also decreases, leading to sediments characterised by more homogeneous, extremely fine sands towards the end of the Younger Dryas. In Figure 26, showing for Syb, the highest sand to silt mass ratio is found at the shallowest, most recent sample while the lowest ratio is found at the opposite side of the dataset.

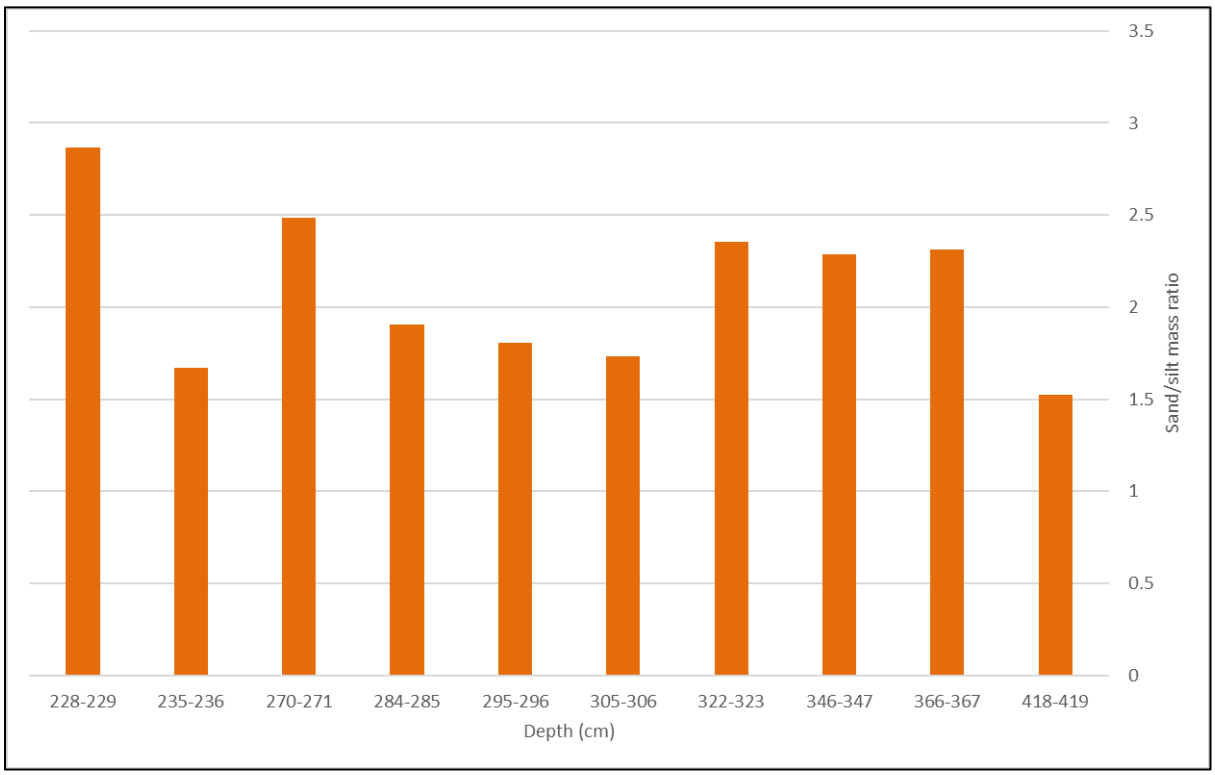

Figure 26 shows the temporal progression of the sand/silt ratio (from right to left) for the 10 samples taken at various core depths of the Syb site expressed in cm on the x-axis.

3.2.2 Ei Van Onnen

A greater degree of variation can be noticed between the sand/silt ratio of the various samples taken in the Ei Van Onnen core when compared to those found in the Syb site, as shown in figure 27. In one case, the mass of the silt component even exceeds the mass of the sand, as seen at the depth of 436-437 cm, in the opposite direction, a distinctly higher ratio of sand to silt mass is observed in the shallowest of the samples. This marks the ultimate moments of the Younger Dryas, where the sand outweighs silt with a sharp 7:1 ratio.

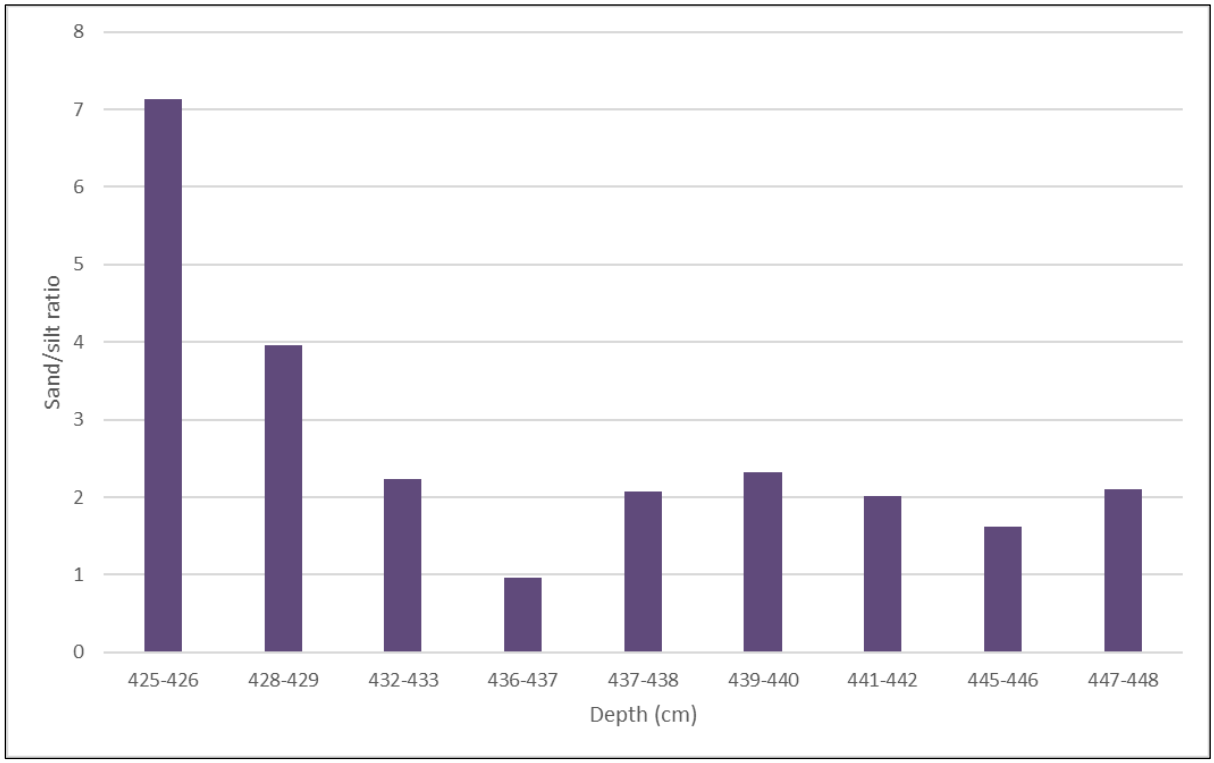

Figure 27 shows the temporal progression of the sand/silt ratio (from right to left) for the 9 samples taken at various core depths in Ei Van Onnen expressed in cm on the x-axis.

3.2.3 Fraeylemaborg

Similarly to the results found for the Ei Van Onnen site, a wide range of values for the sand/silt ratio in the Fraeylemaborg core can be observed. However, unlike the in the Ei Van Onnen case, the sand fraction is never surpassed by the silt mass. The highest sand/silt ratio value again takes place in the shallowest, most recent sample taken with a mass ratio of almost 10:1. The lowest ratio value occurs in the middle of the dataset at 2.859:1 sand/silt mass.

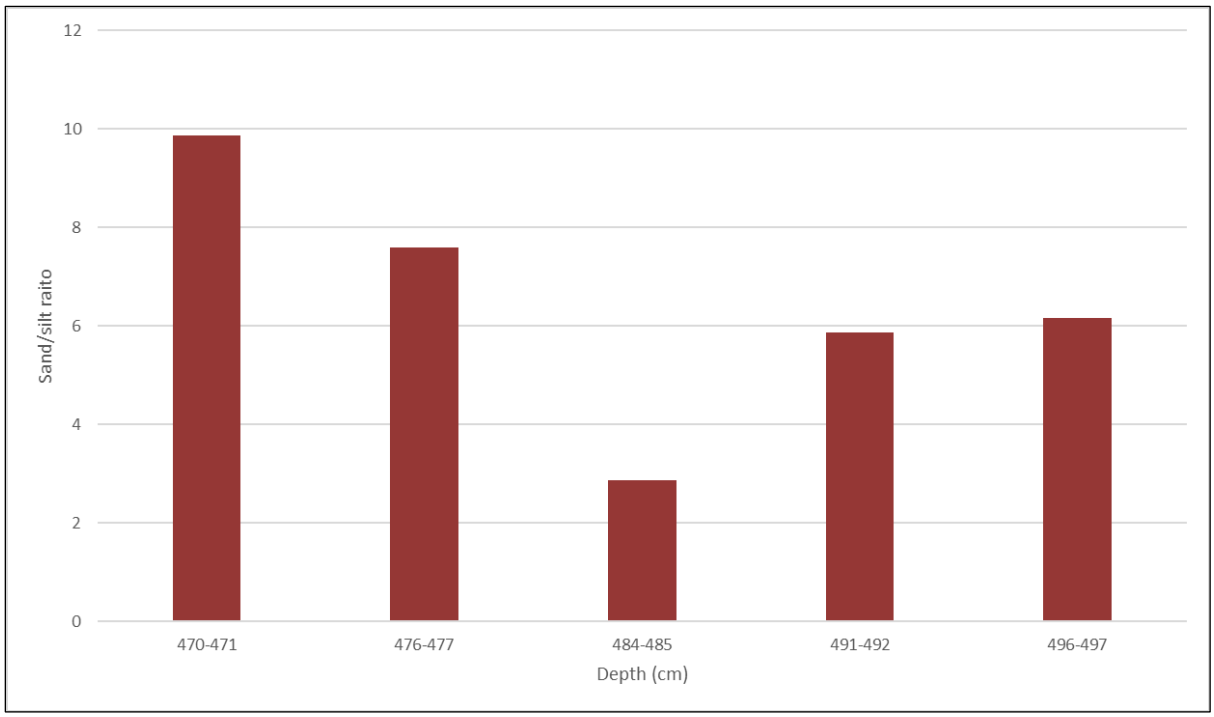

Figure 28 shows the temporal progression of the sand/silt ratio (from right to left) for the 5 samples that have been studied from a range of depths of the Fraeylemaborg pingo remnant core.

3.2.4 Veenklooster

As previously observed in the other 3 pingo sites, the Veenklooster core contains the highest sand to silt mass ratio in the most recent and shallow depth sampled, with a mass ratio exceeding 5 to 1. The deeper sample 20 cm beneath (at 200 – 201 cm below surface) displays a strikingly different scenario, with a much inferior proportional difference at 1.921 between sand/silt.

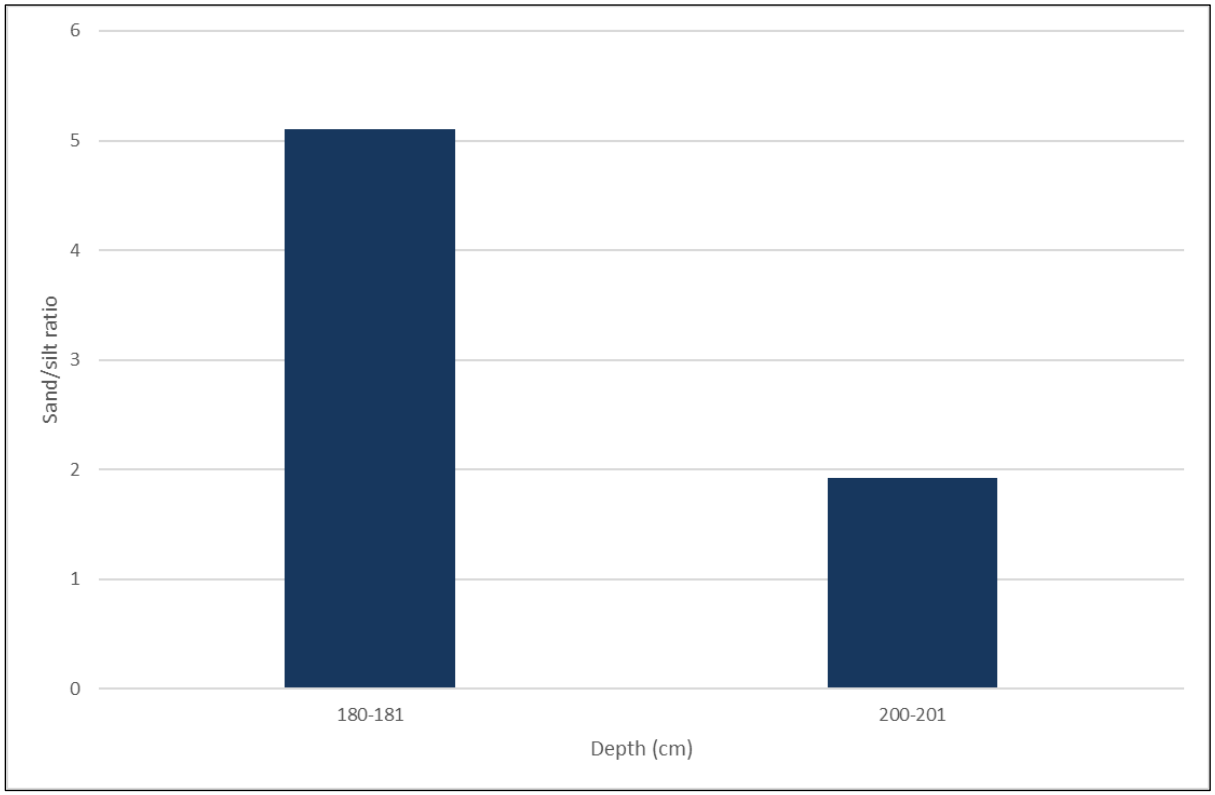

Figure 29 shows the temporal progression of the sand/silt ratio (from right to left) for the 2 samples that have been studied from the depths of 180-181 cm (left) and 200-201 cm (right) of the Veenklooster pingo remnant core.

3.3 Loss on Ignition

This section presents the results obtained by the Loss on Ignition treatment of the samples extracted from the 4 cores respectively attributed to the 4 sites of Syb, Ei Van Onnen, Fraeylemaborg and Veenklooster. The data is presented initially as a simple graph to highlight the fluctuations in the proportion of the inorganic residual mass after the LOI treatment of samples accompanied by two red vertical lines to signify the beginning and end of the Younger Dryas stage. For each of the 4 pingo sites there is a second composite graph that overlaps the LOI results with the pie charts previously shown in section 3.1 to help illustrate the sand distribution based on grain size categories together with histograms showing the median grain size category for sand. The purpose of these visualisations is to provide a wider range of data in the same frame and help contextualise multiple parameters that were observed in this study such as LOI, median grain size and grain size distributions against the time axis.

3.3.1 Syb

The Syb results present with clear distinction the Younger Dryas and Holocene stages as portions with low and high organic content in the sediments, respectively. The Younger Dryas is identifiable between the depths of 223 and 422 cm in the core due to the sharp initial decline on organic content at the beginning (422 cm) and due to the even steeper shift back to organic rich soil seen at the end (223 cm). Before the Younger Dryas, the organic content fluctuates in the 70 – 90 % region followed by a sharp drop to 65% at the beginning of it. Throughout this cold stage the organic content levels decline with a minor peak approximately at the half point (320-325 cm) until it reaches the lowest levels of organic content at the depth of 230 cm with 94% of inorganic residual sediment. Overall, the Younger Dryas aeolian activity in this core has deposited 2 metres of sediment which is followed by the onset of the Holocene which presents extremely prominent levels of organic matter in the sediment, between 95 and 100 %.

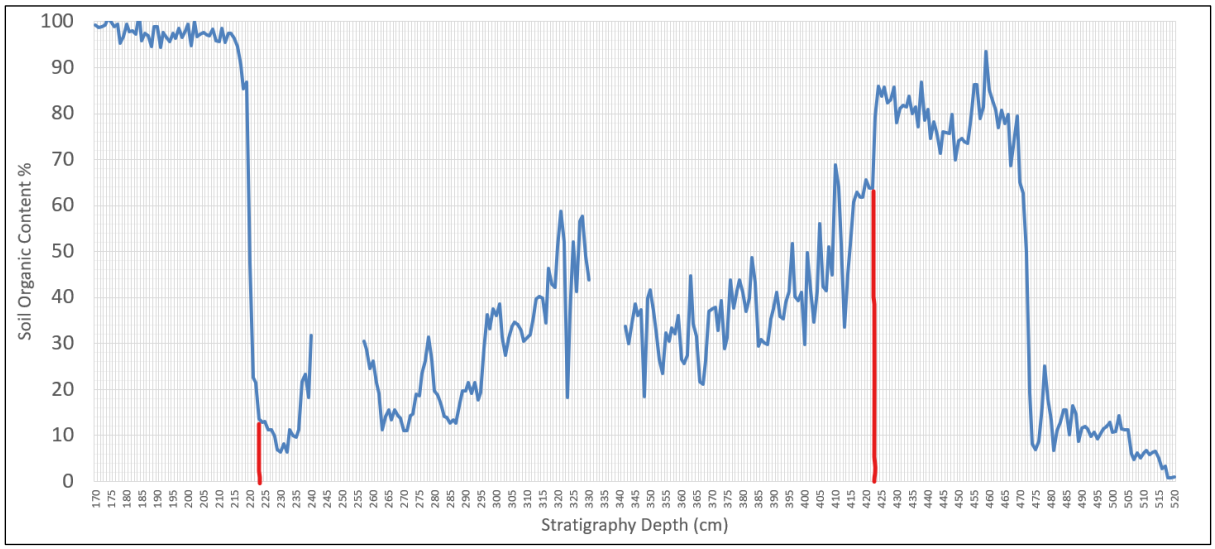

Figure 30. Syb borehole site showing the Loss on Ignition between the depth of 170 and 520 cm, the red vertical lines interpret the onset of the Younger Dryas (422 cm) and the onset of the Holocene (223 cm).

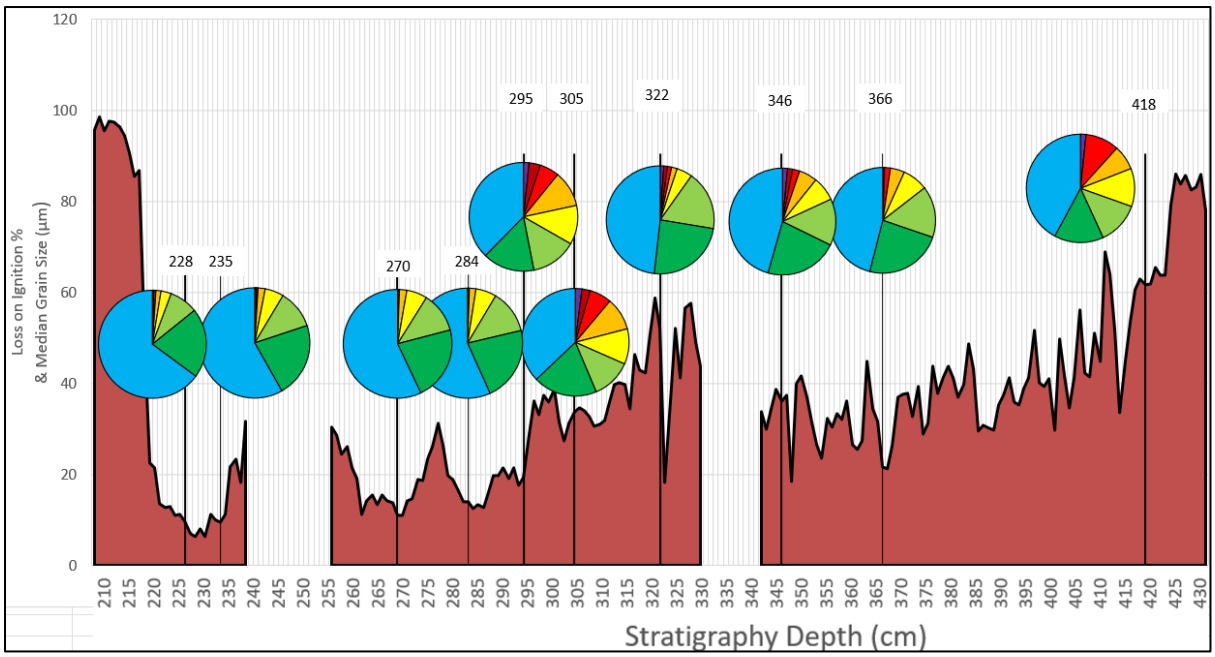

Figure 31. Syb borehole site showing Loss on Ignition versus median grain size for the sands measured. The pie charts display the sand mass distribution according to grain size categories from purple (very coarse sand) to blue (extremely fine sand). The vertical differences in the position of the pie charts are merely to avoid them from overlapping and obstructing the view. The black lines represent the median sand grain size in µm for that particular sample. The numbers on top of each sample indicate the core depth of that particular sample in cm.

3.3.2 Ei Van Onnen

In the Ei Van Onnen results the Bølling–Allerød and Holocene stages are distinguishable as portions with high organic content in the sediments. The Younger Dryas is identifiable between the depths of 425 and 449 cm in the core characterised by lower organic content in the sediments. During the Bølling–Allerød the organic content fluctuates in the 45-60 % region followed by a sharp drop at the beginning of the YD. Throughout this stage the organic content levels decline with two minor peaks approximately at the middle (440 & 436 cm) until it reaches the lowest levels of organic content at the depth of 426 cm with only 5% of organic content detected. Overall, the Younger Dryas aeolian activity in this core has deposited a relatively small amount of sediment which at 24 cm in depth which is followed by the onset of the Holocene. This final stage presents extremely elevated levels of organic matter in the sediment, between 60 and 98 %.

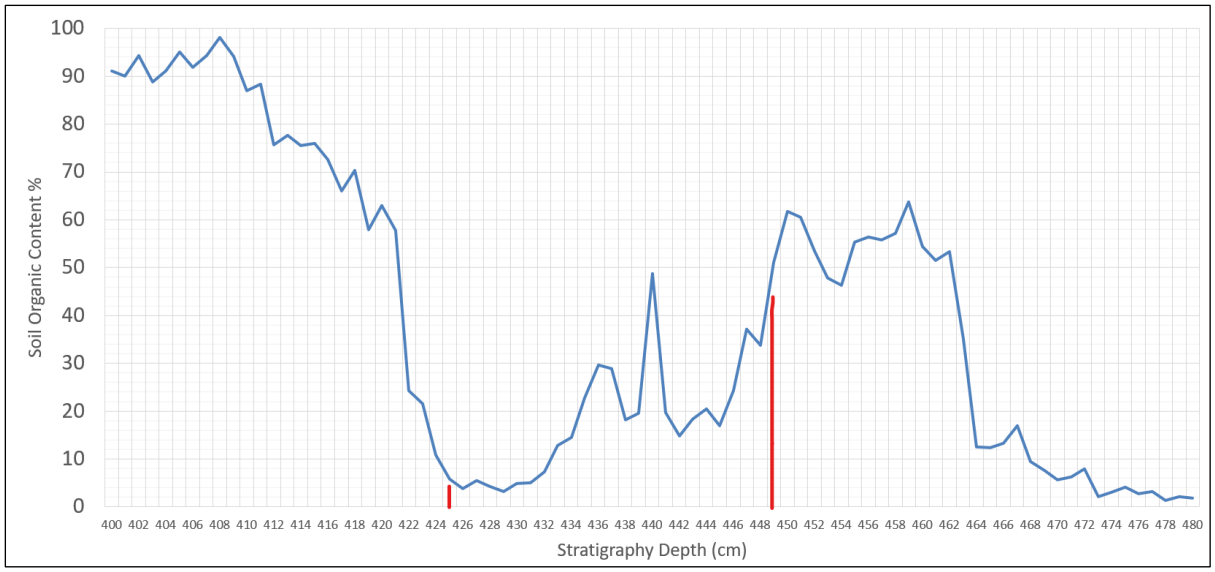

Figure 32. Ei Van Onnen borehole site showing the Loss on Ignition between 400 and 480 cm of depth. The two vertical red lines interpret the beginning and the end of the Younger Dryas at respectively 449 cm and 425 cm of core depth.

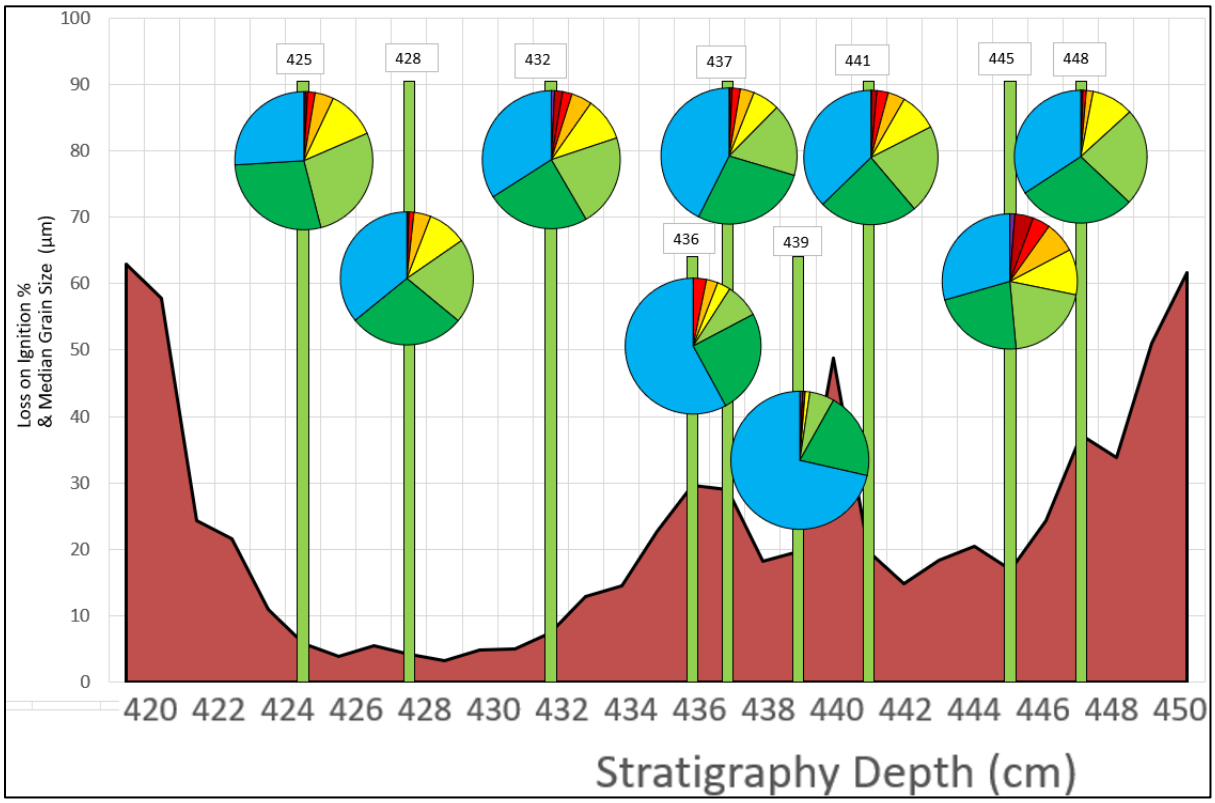

Figure 33. Ei Van Onnen borehole site showing the Loss on Ignition % (black line) vs. median sand grain size in µm (green columns). The numbers labelled on top of each green column indicate the core depth of that particular sample in cm. The vertical position of the pie charts is merely to avoid them from overlapping and obstructing the view.

3.3.3 Fraeylemaborg

For Fraeylemaborg the interstadial section is again equally long as the Younger Dryas stadial part with interstadial LOI values reaching ca 70%, while the Younger Dryas stadial shows values declining from ca 40-5% over almost a 0.9-meter-long interval. The LOI values throughout the Younger Dryas tend to decrease steadily from an organic content level of approximately 30% at the beginning (544 cm depth) to a much lower value of 4% towards the end (469 cm depth).

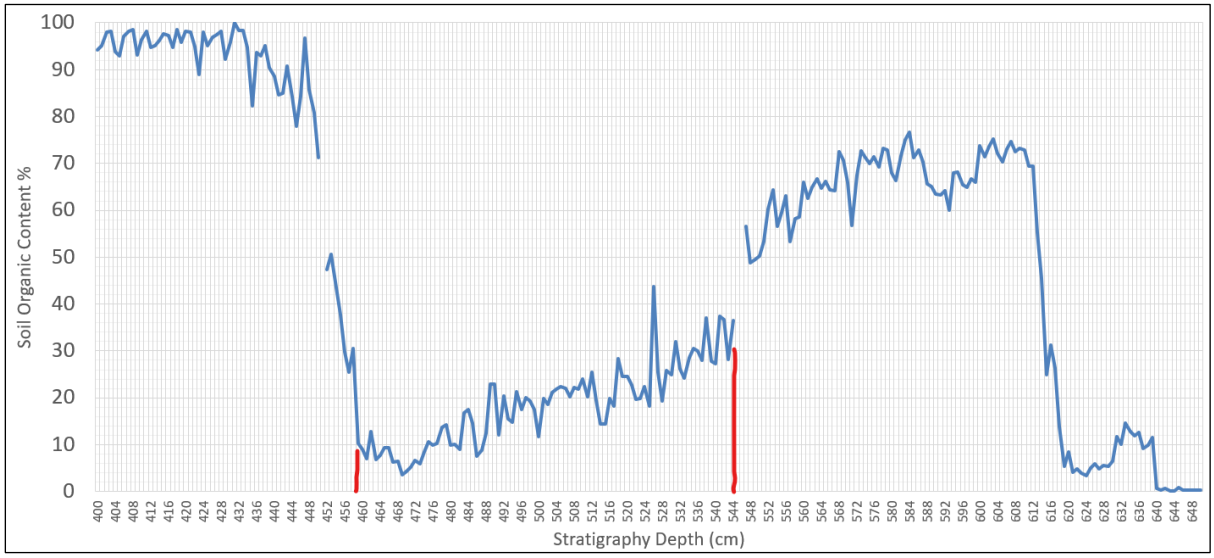

Figure 34. Fraeylemaborg borehole site showing the Loss on Ignition results from 400 to 650 cm of depth. The two vertical red lines interpret the beginning and the end of the Younger Dryas at respectively 544 cm and 458 cm of core depth.

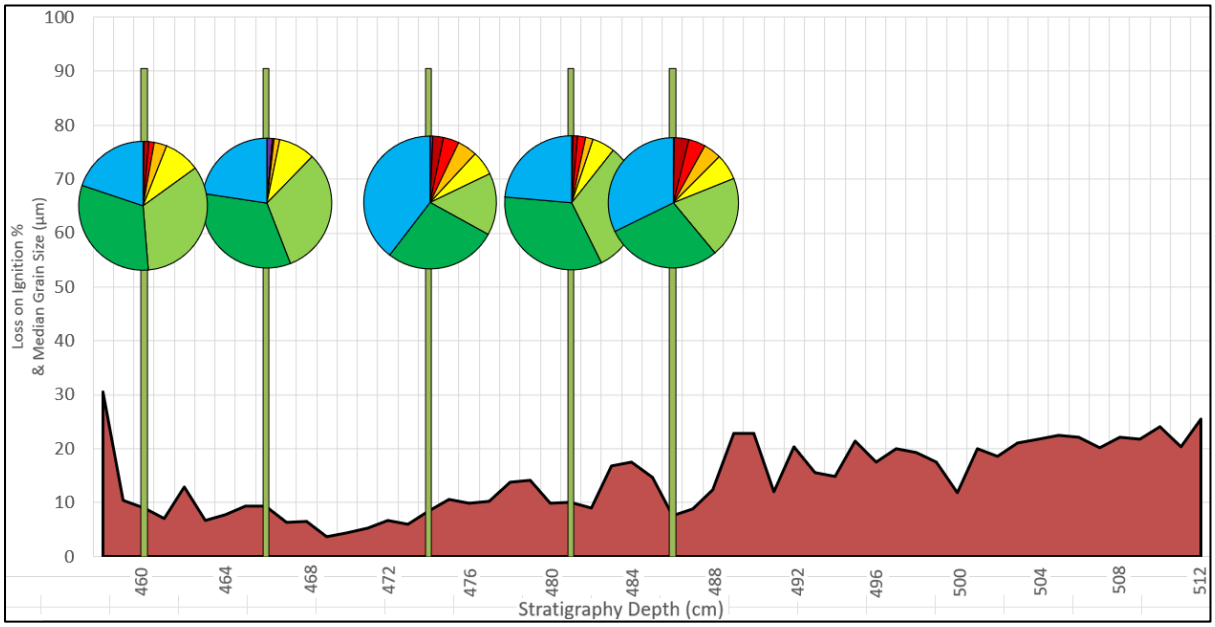

Figure 35. Fraeylemaborg borehole site showing the Loss on Ignition % (black line) vs. median sand grain size in µm (green columns). The vertical position of the pie charts is merely to avoid them from overlapping and obstructing the view.

3.3.4 Veenklooster

For Veenklooster, which was not cored in the centre of the depression, the interstadial part is again equally long as the Younger Dryas stadial part with interstadial organic content values reaching ca 80%, while the Younger Dryas stadial shows values declining from approximately 60-6% over almost a 0.6-meter-long interval. Similarly to the other previous 3 pingo sites, the organic content throughout the Younger Dryas experiences a gradual decline which culminates towards the end, just before the abrupt onset of the Holocene which is characterised by a return in higher organic content levels.

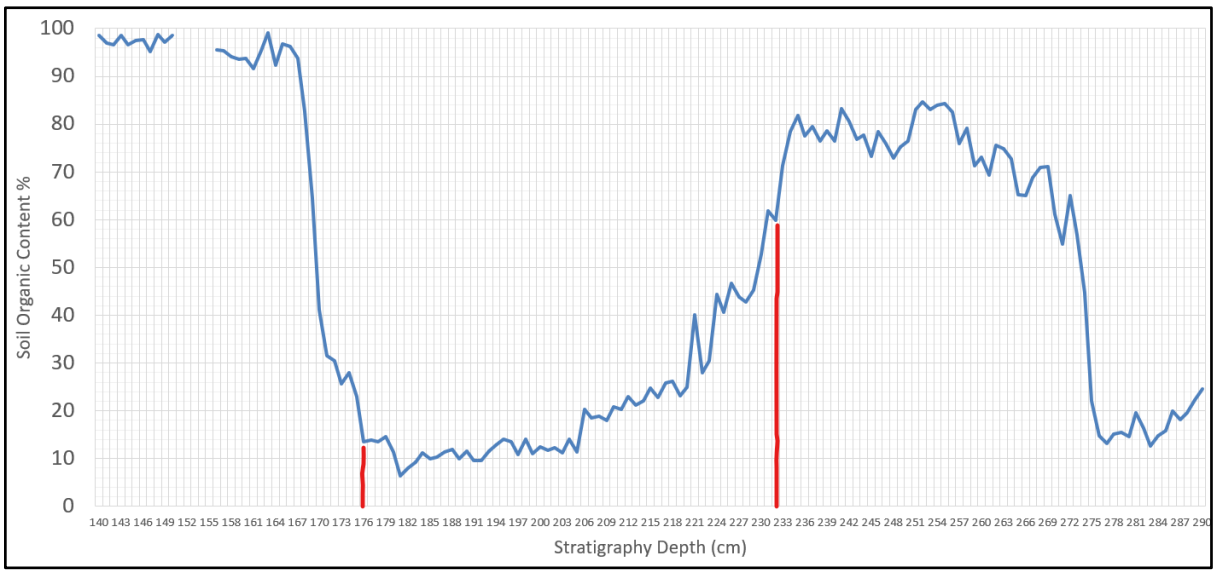

Figure 36. Veenklooster borehole site showing the Loss on Ignition results from 290 to 140 cm of depth. The two vertical red lines interpret the beginning and the end of the Younger Dryas at respectively 232 cm and 176 cm of core depth.

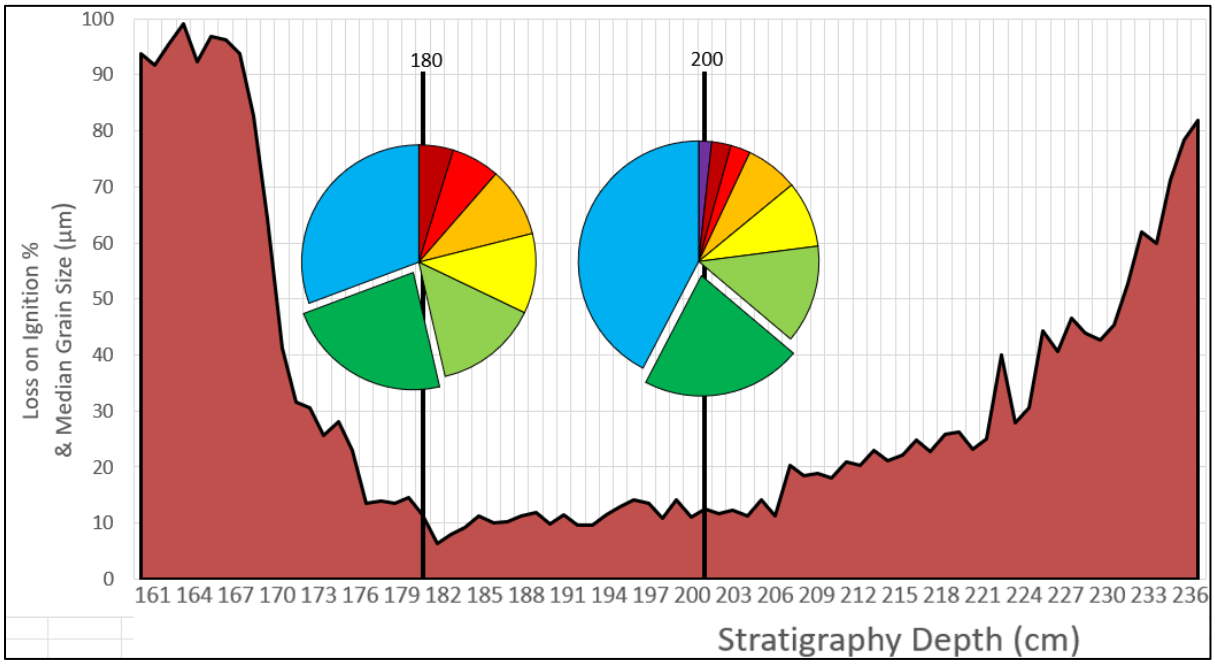

Figure 37. Veenklooster borehole site showing the Loss on Ignition % (black line) vs. median sand grain size in µm (black columns). The portion of the pie chart that is separate from the rest represents the fraction that contains the median sand grain diameter.

3.4 Local Sediment Availability

To answer the question whether the sediments deposited in the pingo fillings are of aeolian origin, the local availability of the same type of aeolian material surrounding the coring site has been looked for. Most importantly, the presence of similar aeolian sediments to the South-West of the 4 borehole sites is expected, as the prevalent winds during the Younger Dryas were blowing from that direction.

3.4.1 Syb

The red circled dots on the figure 38 map show the borehole data that was accessed from DINOloket.nl while the red dot in the centre refers to the borehole that was conducted in the pingo remnant site. Out of the surrounding boreholes, the sediments were compared at the depth of the most recent, uppermost layers of the Boxtel formation (600 - 11.7 ka BP). At such depth is found a less organic-rich layer of fine sand (Younger Dryas) in between two more peaty layers from the previous warmer Allerød oscillation (13.9 - 12.9 ka BP) and the subsequent warmer Greenlandian stage (11.7 - 8.2 ka BP) of the Holocene.

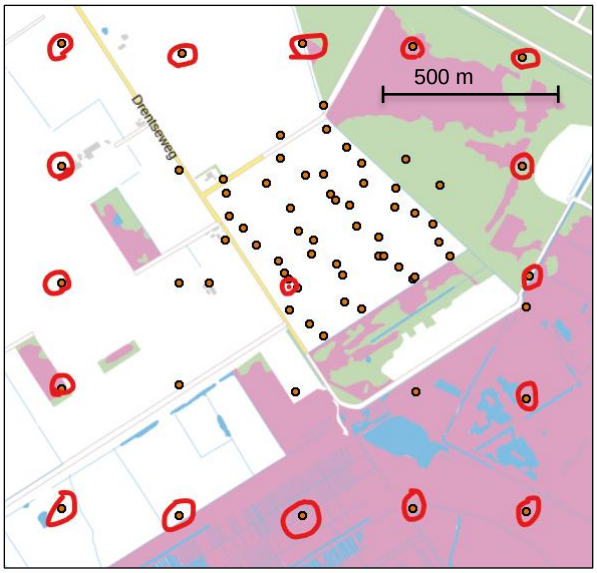

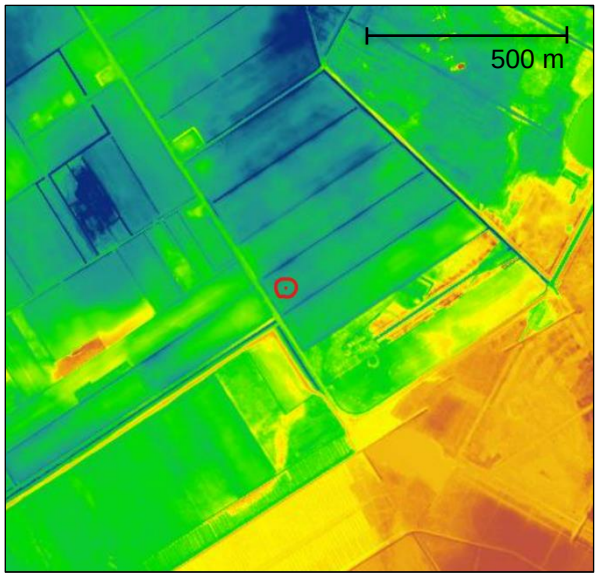

Figures 38 and 39 show the location of the Syb core at the red dot at the centre of the map surrounded by the circled red dots that signal the locations of the surrounding cores used in the comparative study of the sands on the DINOloket database website (left map). The lidar scan data of the ground topography is often used to detect pingo remnants with the AHN Viewer mapping software (right map) and it shows the location of our Syb core indicated in red.

Table 6 shows the code names of the cores (left column) used for the comparative study of the sands, with the relative directions to our core site (centre column) expressed for practical purposes and finally the median sand grain size in µm of the sands found in the depths recognised as the Boxtel Formation (right column). The rows highlighted in green contain sands with median grain diameters considered the most similar to the ones measured in the Younger Dryas sands of our core.

Syb Surrounding Boreholes	Relative heading to pingo coring	Sand Grain Median Size (micron)
B12C1305	NW	>2000 “sand”
B12C1308	NWN	160 “sand”
B12C1311	N	120-140 “sand + silt + gravelly”
B12C1313	NEN	100-160 “sand + silt”
B12C1316	NE	130-150 “sand + silt
B12C1317	ENE	80-150 “sand + silt + gravel”
B12C1318	E	145-150 “sand + silt + gravel”
B12C1226	ESE	150 “sand + gravel”
B12C1227	SE	160 “peat + sand + silt + gravel”
B12C1224	SES	155 “sand”
B12C1221	S	N/A “peat”

Syb Surrounding Boreholes	Relative heading to pingo coring	Sand Grain Median Size (micron)
B12C1305	NW	>2000 “sand”
B12C1218	SWS	N/A “peat”
B12C1215	SW	N/A “peat”
B12C1214	WSW	150-155 “sand + gravel”
B12C1307	W	155 “sand + gravel”
B12C1306	WNW	160 “sand + gravel”

Table 7 shows the depths (left column) of the samples taken in the Syb core and their sand median grain size (right column) that were calculated.

Syb Core Depth (cm)	Sediment Median Sand Diameter (micron)
418-419	75 - 106
366-367	75 - 106
346-347	75 - 106
322-323	75 - 106
305-306	75 - 106
295-296	75 - 106
284-285	53 - 75
270-271	53 - 75
235-236	53 - 75
228-229	53 - 75

3.4.2 Ei Van Onnen

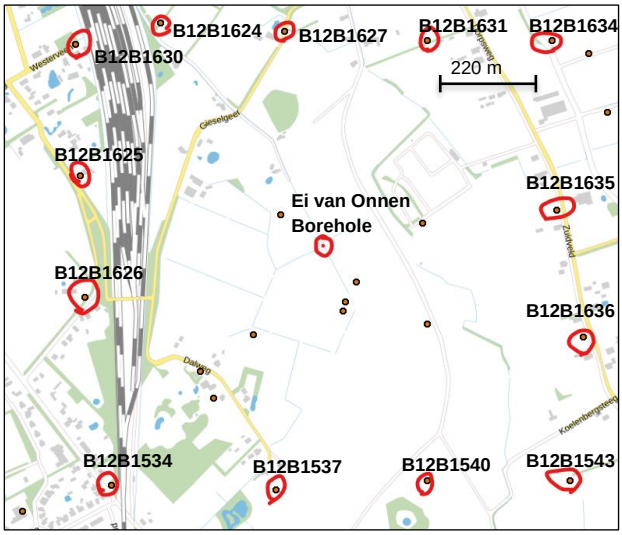

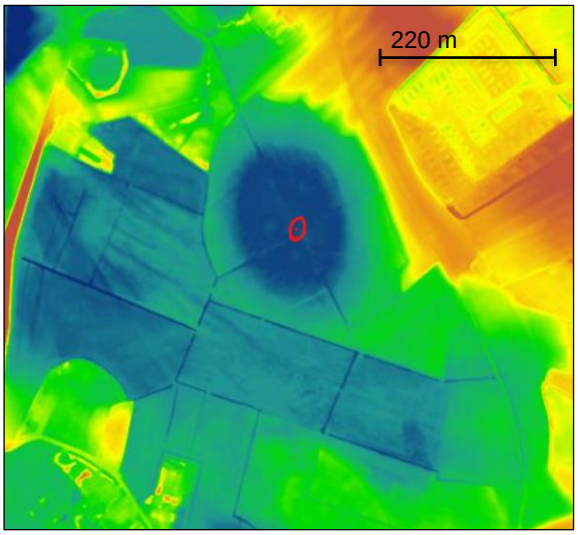

Figures 40 and 41 show the location of the Ei Van Onnen core at the red dot at the centre of the map surrounded by the circled red dots that signal the locations of the surrounding cores used in the comparative study of the sands on the DINOloket database website (left map). The codes in the left map are the names of the surrounding boreholes from the DINOloket database. The lidar scan map with the AHN Viewer mapping software (right map) shows the location of the Ei Van Onnen core indicated in red.

Table 8 shows the code names of the cores (left column) used for the comparative study of the sands, with the relative directions to the Ei Van Onnen core site (centre column) expressed for practical purposes and finally the median sand grain size in µm of the sands found in the depths recognised as the Boxtel Formation (right column). The rows highlighted in green contain sands with median grain diameters considered the most similar to the ones measured in the Younger Dryas sands of the EVO core.

Ei Van Onnen Surrounding Boreholes	Relative heading to central borehole	Sand Median Grain Size (micron)
B12B1630	NW	N/A “sand”
B12B1624	NWN	N/A “sand”
B12B1627	NWN	150 “sand and gravel”
B12B1631	NEN	155 “sand”
B12B1634	NE	150 “sand + 10% silt + gravel”
B12B1635	ENE	160 “sand”
B12B1636	ESE	155 “sand”
B12B1543	SE	145 “sand”
B12B1540	SES	135 “sand”
B12B1537	SWS	150 “sand”
B12B1534	SW	150 “sand”
B12B1626	WSW	160 “sand”
B12B1625	WNW	165 “sand”

Table 9 shows the depths (left column) of the samples taken in the EVO core and their sand median grain size (right column) that we calculated.

Ei Van Onnen Core Depth	Median Grain Sand Diameter (micron)
447-448	75 - 106
445-446	75 - 106
441-442	75 - 106
439-440	53 - 75
437-438	75 - 106
436-437	53 - 75
432-433	75 - 106
428-429	75 - 106
425-426	75 - 106

3.4.3 Fraeylemaborg

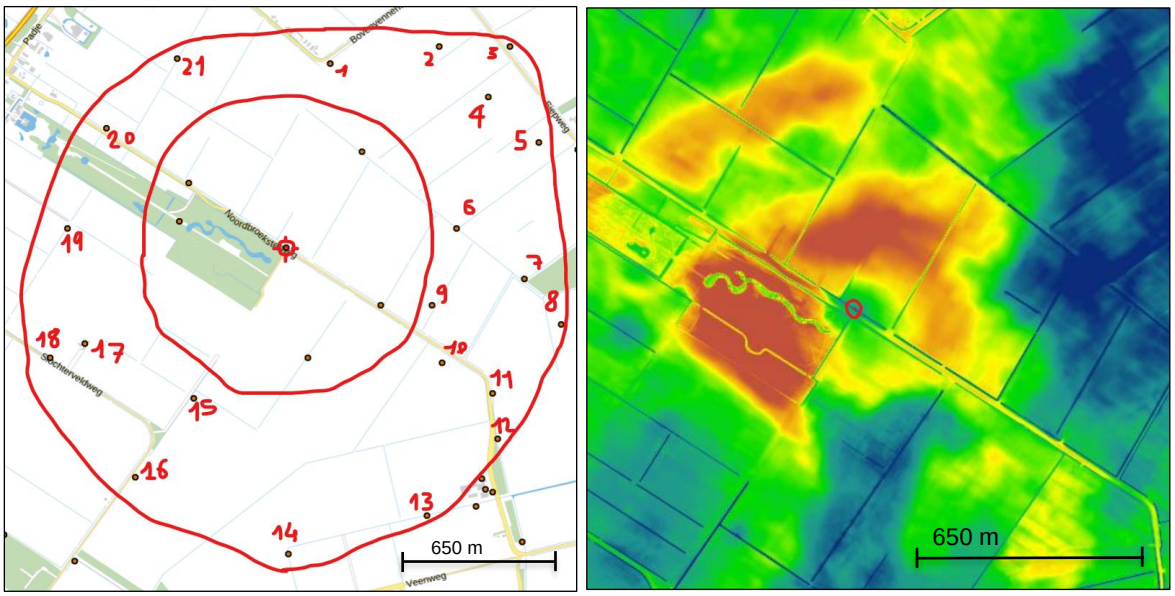

Figures 42 and 43. Show the location of the Fraeylemaborg core at the red dot at the centre of the map surrounded by the 21 numbered dots that signal the locations of the surrounding cores used in the comparative study of the sands on the DINOloket database website (left map). The lidar scan map from the AHN Viewer mapping software (right map) shows the location of the Fraeylemaborg core indicated in red.

Table 10 shows the code names of the cores (left column) used for the comparative study of the sands, with the relative directions to the Fraeylemaborg core site (centre column) expressed for practical purposes and finally the median sand grain size in μm of the sands found in the depths recognised as the Boxtel Formation (right column). The rows highlighted in green contain sands with median grain diameters considered the most similar to the ones measured in the Younger Dryas sands of the Fraeylemaborg core.

Fraeylemaborg Surrounding Boreholes	Relative heading to central borehole	Sand Median Grain Size (micron)
B07H0814	NEN	130 - 160 “sand + silt”
B07H0817	NEN	N/A “sand”
B07H0821	NE	145 - 185 “sand + silt + gyttja”
B07H0818	NE	165 - 185 “Gyttja + sand”
B07H0771	ENE	N/A “sand”
B07H0762	E	160 - 165 “sand”
B07H0769	E	150 “sand + peat”
B07H0772	ESE	N/A “sand”
B07H0765	ESE	Medium to fine “sand”
B07H0709	SE	N/A “sand”
B07H0706	SE	170 - 165 “sand”
B07H0710	SE	N/A “sand”
B07H0705	SES	155 - 165 “sand”
B07H0708	S	155 - 170 “loam + sand + silt + gyttja”
B07H0703	SW	155 - 180 “loam + sand + silt + gravel
B07H0702	SW	100 - 145 “sand”
B07H0120	WSW	N/A “loam”
B07H0701	WSW	120 “sand + gravel”
B07H0760	W	155 - 165 “sand”
B07H0758	WNW	100 - 155 “sand”
B07H0812	NWN	150 - 185 “sand + gravel + silt”

Table 11 shows the depths (left column) of the samples taken in the Fraeylemaborg core and their sand median grain size (right column) that we calculated.

Fraeylemaborg Core Depth	Median Grain Sand Diameter (micron)
496-497	75 - 106

491-492	75 - 106
484-485	75 - 106
476-477	75 - 106
470-471	75 - 106

3.4.4 Veenklooster

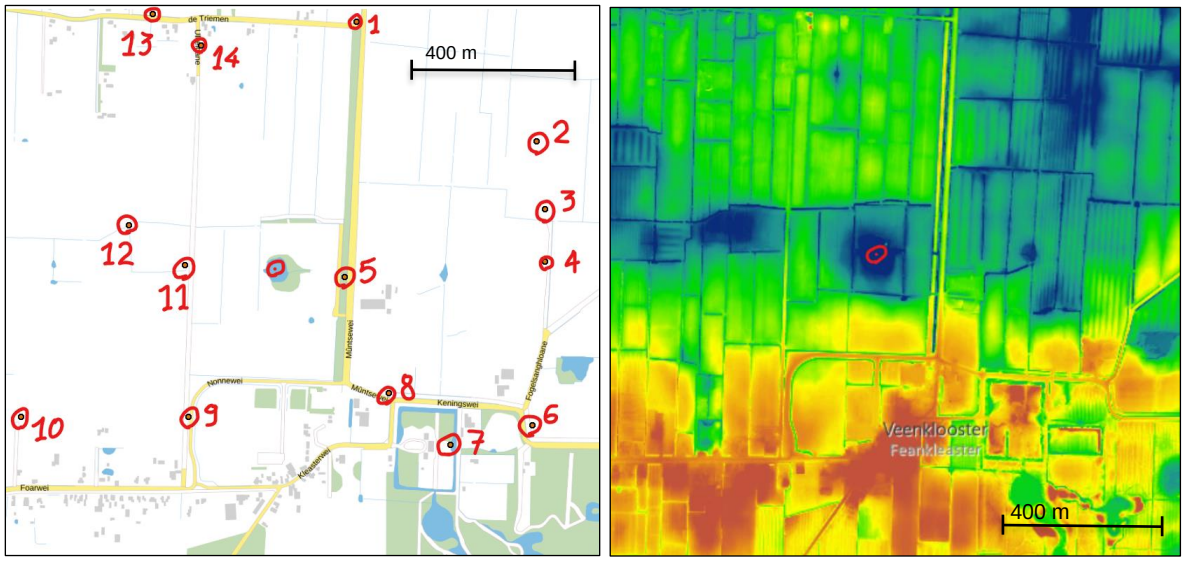

Figures 44 and 45 show the location of the Veenklooster core at the red dot at the centre of the map surrounded by the 14 numbered dots that signal the locations of the surrounding cores used in the comparative study of the sands on the DINOloket database website (left map). The lidar scan map from the AHN Viewer mapping software (right map) shows the location of the Veenklooster core indicated in red.

Table 12 shows the code names of the cores (left column) used for the comparative study of the sands, with the relative directions to the Veenklooster core site (centre column) expressed for practical purposes and finally the median sand grain size in µm of the sands found in the depths recognised as the Boxtel Formation (right column). The rows highlighted in green contain sands with median grain diameters considered the most similar to the ones measured in the Younger Dryas sands of the Veenklooster core.

Veenklooster Surrounding Borehole	Relative heading to central borehole	Sand Median Grain Size (micron)
B06E0247	NEN	155 - 165 “sand + gravel”
B06G1198	NE	N/A “sand”
B06G1199	ENE	110 - 250 “sand + gravel + loam + lutum”
B06G1197	E	N/A “sand”
B06G1200	E	N/A
B06G1141	ESE	N/A “sand”
B06G0089	SE	N/A “sand + silt”
B06G1140	SE	120 - 155 “sand + gravel”

B06G1139	SWS	150 - 160 “sand”
B06G1136	SW	N/A “sand + loam”
B06G1194	W	145 - 155 “sand”
B06G1196	WNW	N/A “sand”
B06E0111	NWN	N/A “sand”
B06E0245	NWN	160 - 145 “sand + silt”

Table 13 shows the depths (left column) of the samples taken in the Fraeylemaborg core and their sand median grain size (right column) that we calculated.

Veenklooster core Depth	Median Sand Grain Size (microns)
200-201	75 - 106
180-181	75 - 106

4. Discussion

This section focuses on the interpretation of the parameters measured in the study and connects the findings with the three research sub-questions that define this project. The results are also contextualised with previous knowledge from other research to observe if they link with other works of Dutch climate reconstruction or if there are contradictions.
The expectations, based on previous studies is to find that the deposition of aeolian sediment increases gradually throughout the Younger Dryas, as the seasonal winds became stronger and the weather stormier. Other results expected include a general heterogenization of the sand distribution by grain diameter due to stronger wind forces taking place in the latter half of this stage. Thirdly, the general expectation is to find that the sand to silt mass ratio increases with time due to the increasing proportion of coarser sand being transported by aeolian forces. These expectations rely on a simplified understanding of the wind and climate in general, meaning that anomalies are not necessarily symptom of an improper method of investigation because they reflect storm events, vegetation changes, fluctuations in the seasonal winds and sediment availability through time.

4.1 Loss on Ignition

The results acquired on the Loss on Ignition residuals generated similar graphs across all four pingo remnant sites assessed. All sites present prominent levels of organic content before and after the Younger Dryas stage. This implies that surrounding vegetation in these warmer periods of time was likely denser and more productive. This is reflected in the stratigraphical record where the presence of more woodland vegetation coincides with warmer and wetter climate conditions, according to previous palynological research (Hoek, 1997). The 2 stages of higher organic content, coincide with the Bølling–Allerød interstadial which occurred before the Younger Dryas between 14.7 - 12.9 ka BP and the onset of the Holocene at 11.72 ka BP (Rasmussen et al., 2006).

The increase in residual proportion found in the samples from the Younger Dryas is explained by a gradual decrease in the general productivity of the vegetation which in turn limited the energy available for the entire ecosystem. Palynological evidence also strongly supports the claim that vegetation was much more developed in the Netherlands before and after the Younger Dryas stage. Pollen analysis shows that a decrease in the genus *Pinus* (pine) took place quickly after the onset of the Younger Dryas, while herbaceous species took over as the main type of vegetation covering the landscape (Hoek, 1997).

4.2 Climate, Vegetation & Geomorphology

The disappearance of pine forests is considered the principal driver for the increase in aeolian sand deposition across the country, because grasslands offer less protection to the soils against aridification and erosion than forests do. Previous studies have in fact measured a substantial increase in aeolian sand deposition, with a minor lag after the pine forests disappeared (Hoek, 1997). Such non-arboreal plants took over the landscape, as observed in the changes in the proportion of non-arboreal to arboreal pollen counts obtained from core samples of the Younger Dryas stage. Due to the increased vulnerability of soils to aeolian processes and the

overall decrease in vegetation biomass, the Younger Dryas is easily identified across the LOI graph because it is characterised by very high percentages of inorganic content for its soil.
By factoring together all the processes mentioned, there appears to be a strong link between the climate changing, which affects the vegetation cover, which in turn influences the surface geomorphological features (Hoek and Bos, 2018).
This connection between Earth's climate, the vegetation and geomorphology means that by looking at the LOI, researchers can interpret the fluctuations that these three environmental parameters experienced throughout the Younger Dryas.

4.3 The YD - PB Transition

A characteristic universal finding to the LOI data found in all four pingo remnant cores, is that the ending of the Younger Dryas was very abrupt, this concords with other publications which claim that in a matter of simple decades, the arid and cold millennium abruptly ended (Cheng et al., 2020).
With the onset of the Holocene, results show very high levels of organic content, generally fluctuating in the 90-100 % region. Unsurprisingly, the Greenlandian (or Pre-Boreal) stage of the Holocene was characterised by an abrupt increase in tree pollen throughout the palynological record and an increase in organic matter content, without a lag (Hoek, 1997).
With the conclusion of the Younger Dryas, the Netherlands experienced an increase in temperatures by 5 to 8 degrees Celsius in a matter of years. This factor contributed to the return of arboreal vegetation cover, but also for a 14% increase in annual rainfall and a 60% decline in snowfall (Renssen, 2001).

As mentioned earlier, vegetation density strongly influences the geomorphology, in fact, with the return of arboreal species, the topsoil became less vulnerable to aeolian erosion. To complement this, the annual days characterised by strong winds, declined to just a quarter of the amount taking place in the Younger Dryas (Renssen, 2001).
Immediately after the Holocene onset, 11.7 ka BP, our LOI results have a stable appearance, however the Pre-Boreal climate was not exactly identical to that of the modern-day Netherlands. The subtle difference was that the early-Holocene was characterised by a wider range of seasonal temperatures, which contributed to slightly more snowfall, humidity, colder winters and warmer summers. This situation was mainly caused by two factors which differ than today's situation, the first is the presence of partial ice cover located in the North Atlantic, which mitigated the warming characteristic of the AMOC for the European continent. The second factor is astronomical climate forcing, caused by orbital resonances between Jupiter, Earth itself and Venus. In turn these resonances alter the shape of Earth's orbit around the Sun, which caused the solar insulation levels during the pre-boreal to be 30 watt/m^2 higher during the summer and 10 watt/m^2 weaker in winter relative to present day (Renssen, 2001).

4.4 The Younger Dryas LOI Peak

All but the Veenklooster pingo remnants, present in their LOI levels, a central peak of higher organic soil content generally at the half point of the sediment record for the YD. This curious feature is most prominent in the Syb core despite some gaps in the data, still distinct in the EVO core and barely noticeable in the Fraeylemaborg site. Due to the geographical alignment of the

three sites that present this intermediate peak in organic content, it is intuitive to assume a connection with the seasonal wind due to its South-Westerly direction in the summer months (Kasse et al., 2020). On top of that, the gradual weakening of the signal along the natural progression of the wind path (from Syb to EVO to Fraeylemaborg) is another clue that perhaps this was a small-scale fluctuation in aeolian sediment deposition. On one side, it is easy to assume that the cause for this anomaly may be a localised variation in either wind strength or sediment availability. Through the observation of the LOI data another possibility emerges: the three aligned pingo remnant sites show an intermediate LOI peak during the middle of the Younger Dryas. In this circumstance there is a risk of misinterpreting different signals as having the same cause of origin, especially due to the noise in the data produced by the natural fluctuations of the environment and due to measurement error. The weakness in this interpretation is the lack of a higher amount of pingo remnants being investigated in the same exact methods. This would otherwise offer a statistically stronger foundation to base assumptions on.

4.5 Sediment Availability Interpretation

Pingo remnants experience different sedimentation rates, which in turn, fluctuate across time. As a matter of fact, we observe that the duration of the YD is very different across the stratigraphy our four core sites. In Syb (Fig. 30) the YD produced approximately 2 metres of sediments, while in EVO (Fig. 32) the YD produced only about 24 cm of layers. The sedimentation rates vary to a high degree, which makes the job of connecting dips and peaks between multiple sites, a risky but sometimes insightful work. In figure 34 we measure that the duration of the YD at the pingo site in Fraeylemaborg deposited 86 cm of sediments while the pingo of Veenklooster saw 56 cm of sediments throughout that window of time (Fig. 36).

The vast differences in the sedimentation rate of these pingos tells us that in the Northern Netherlands, there was a strong spatial variability among the locations that experienced aeolian sedimentation. What emerges, is a fascinating result, which falls in line with the outcome of the study that reconstructed the South-Westerly seasonal wind (Kasse et al., 2020) The result is that Syb, the first of the three aligned locations to receive the seasonal summer wind, did in fact receive the highest amount of aeolian sediments of all sites. Ei Van Onnen located precisely North-East, 22 km downwind of Syb, experienced a sedimentation rate that was just 12% of the one in Syb. This could indicate that between the two locations, very few sand deposits were present for the winds to transport and deposit in the EVO pingo lake. The second indicator that sand deposits were spread unevenly across the Northern Netherlands is that Fraeylemaborg, just 14 km North-East to Ei Van Onnen, experienced a sedimentation rate >3 times as great as measured in Ei Van Onnen. The results suggest that an abundant quantity of sand deposits must have existed along the imaginary line that connects Ei Van Onnen with Fraeylemaborg, and on the contrary, between Syb and EVO, the availability of aeolian sediments was scarce.
The assumptions are plausible but remain constrained within the limitation that the prevalent, south-westerly seasonal wind was not significantly influenced by others from different directions. Furthermore, local presence of available sand is the most important prerequisite.

4.6 Sediment Comparison with a DINOloket.nl Online Database

Thanks to DINOloket.nl, users can gather insights on the sediment availability of the area surrounding any pingo remnant site in the Netherlands. The database is a library of information based on the coring work of previous research projects from third parties.

4.6.1 Syb

At the Syb pingo remnant, 17 cores within the surrounding 2 km^2 have been investigated (table 6). The results are sometimes incomplete or lack sufficient stratigraphical resolution, but most of the surrounding sites contained sand ranging between 80 and 160 μm in median diameter, often accompanied by some gravel. Most surprising was the discovery that the 3 sites which were found South, South-West-South and South-West of our core location, did not contain high levels of sand. Their layer associated with the Boxtel formation, which is the layer of sediment that extends from 600 ka BP to 11.7 ka BP, was categorised as “peat”. This result contrasts the very high proportion of aeolian soil that characterises the pingo filling at Syb. Such unexpected result could be due to a wrong interpretation of the sediment by part of the third party that executed the coring work in the surrounding area of the Syb pingo. Another possibility is that in this case the source of aeolian sand might have been located further downwind and that the specific locations for the cores B12C1221, B12C1218 and B12C1215. Such sites lack detailed information and could have been compromised by agricultural activity in the most recent decades. The other directions surrounding the Syb borehole could have been sources of aeolian sediment from the Younger Dryas, with sands of mean diameter slightly greater (80-160 μm) than those measured in the pingo remnant (53 - 106 μm) as shown in table 7. It is expected to find a slightly inferior grain size with the in-blown sediments when compared to those at the source. This is due to the fractionation process occurring with wind speeds that, similarly to fluvial transportation, manage to carry particles up to a certain size limit, imposed by the velocity of the channel current or wind.
In the Syb site, there is a general decrease in median grain size across the progression of the Younger Dryas according to the pie charts in figure 31 and table 7. The pie charts show a distribution of the grain sizes sorted by colours. We notice a gradual shift across the YD where the sand distribution by grain size becomes homogenised, due to the coarse and medium sands composing a smaller mass fraction of the total sample. At the very end phase of the YD, almost 60% of the sample mass is made of the finer half of extremely fine sands (75 - 53μm). This outcome contrasts the general understanding that the YD gradually became windier and stormier, if this were the case, we would observe a coarsening of the sands instead. It is possible that the characteristics of the sediment available may have changed which would cause the aeolian deposits to become finer despite the increasing wind speeds.

4.6.2 Ei Van Onnen

At the Ei Van Onnen site (table 8) the surroundings (table 9, figure 40) show that from all directions, there is aeolian sediment available from the upper layers of the Boxtel formation. These sands are generally coarser than in Syb, with a tighter, more homogeneous range of

median grain sizes oscillating between 165 and 135 μm. At this pingo remnant, our core data reveals similar sand median grain diameters, although this time, the samples with the median range of 53 - 75 μm are located broadly in the centre of the YD stratigraphy, while in Syb those were concentrated at the end of it. Surprisingly, despite the more homogenised sediments available around EVO, the pie charts reveal a more heterogeneous composition across time than for the Syb core. As expected, the two samples with the finest median grain size are the least heterogeneous across grain size categories. Notably, the older of the two, found at 439-440 cm of depth is so homogeneous that almost 75% of its mass is made of sand particles smaller than 75μm. An anomalous peak of sediment rich in organic content is located just a few cm below this sample, which could indicate a temporary decline in wind speed due to a short-lived resurgence of larger vegetation. This situation would only allow for the finest sands to be lifted by aeolian transport and deposited into the pingo lake.
Overall, the EVO core appears with a constant, heterogenous sand composition from the start to the end of the Younger Dryas, characterised by some anomalous oscillations towards the middle.

4.6.3 Fraeylemaborg

At Fraeylemaborg (figures 42-43) (tables 10-11), 21 cores surrounding the site were studied. Sand was almost always found, with appearances of gyttja, loam and high concentrations of silt. The median sand grain sizes have a broader range than EVO, moving between 100 to 185 μm, contributing to a rather heterogeneous type of sediment. Notably, the finest sands found in South-West and West-North-West facing boreholes appear as the potential sources of aeolian sediment that today characterises the pingo filling. This finding concords with the median sand grain sizes (75 - 106 μm) measured in 5 samples of the Fraeylemaborg core. When observing the overlap of the sand distribution pie charts with the LOI data we notice a slight trend whereas the YD progresses, the organic content diminishes, and so does the fraction of coarse sand (bright red, dark red and purple fractions) found to be larger than 300μm from our sieving work. An example of how closely linked the LOI and the presence of coarse sand is the fact that the sample at 491 cm of depth has an organic content of 12.5% while the previous and subsequent samples have an organic content of 17%. Following this same pattern, it becomes easy to glance that those two adjacent sites also happen to contain a greater proportion of coarse sands.
This correlation between organic content and coarser sand contradicts the general assumption that with increasing aridity and wind, the aeolian deposits shall become coarser. This counterintuitive scenario presents to us a generally constant median grain size but a proportion of coarse sand that reflects the trend observed for the proportion of inorganic content.

4.6.4 Veenklooster

In the Veenklooster core site (figures 44-45) (tables 12-13), 14 cores from the surroundings have been studied. Aeolian sand is almost always detected with sporadic detection of loams and lutum while the median sand grain size ranges from 110 up to 250 μm. The interpretation of this region is that the aeolian deposits are quite heterogeneous, but a limitation arises due to 8 of the cores lacking the measurement of the median sand grain size. The inconsistency of the core depths and interpretations of the data can noticeably weaken the effectiveness of a study

that relies on comparing fresh results with ones from a third-party online database. A glance at figure 31 shows a trend opposite to what has been noted so far from the Syb and Fraeylemaborg, the aeolian deposits are coarser towards the end of the Younger Dryas. In specific, the portion of the finer half of the extremely fine sand (53-75μm) experiences a moderate decrease, giving new space to the coarser categories of sand (300-425μm and 425-600μm). The green and yellow proportions are less affected, while the complete disappearance of the purple (>600μm) category hints that it may be caused by the random presence of a handful of very coarse sand grains. Either way the results this time concord with the assumption of the Younger Dryas experiencing more extreme weather storms towards the end of its duration, which would drive a more heterogeneous and coarse mixture of aeolian sediments to deposit at the bottom of the Veenklooster pingo lake.

4.7 Effects of The Younger Dryas on the Organic Content

Overall, for the loss on ignition results, there is a stark difference in the inorganic residual content between the stadia that took place before and after the Younger Dryas. The data shows that the Bølling–Allerød interstadial was identified by soil organic contents ranging from 48 - 85% while the Pre-Boreal stage was characterised by organic content almost reaching 100%, a result that concords with our visual assessment of peat during the Syb core fieldwork. Throughout the Younger Dryas, the LOI results indicate levels of inorganic contents as high as 96% in Ei Van Onnen and Fraeylemaborg and 94% in Syb and Veenklooster. All pingo remnants exhibit such peak in inorganic content, in proximity to the termination of the Younger Dryas, suggesting that the climate was gradually turning harsher for plant life right until the abrupt onset of the Holocene.

How sandy was the Younger Dryas in comparison to the Bølling–Allerød and the Pre-Boreal? The Younger Dryas was distinctively sandier than the previous and subsequent stages, because our data shows that the soils experienced a loss of 42 - 81% of their organic component between the end of the Pre-Boreal and the end of the Younger Dryas. The YD termination presents an even greater leap of change of the soil composition, which experienced an increase of organic content by as much as 95% in the span of a few decades. Wind speeds also declined by approximately 20%, mainly due to the climate change but aeolian transport diminished also due to the resurgence of pine forest cover across the Northern Netherlands (Hoek, 1997) (Renssen, 2001).

4.8 Reconstructing Wind Speed & Direction

The knowledge about the sand/silt ratio for a particular depth of a core, can improve our understanding of the wind conditions at a location thanks to the small nature of silt particles. Due to their inferior diameter to sand, silts are more prone to aeolian transportation under light wind speeds. This means that an increase in sand/silt ratio through the stratigraphy of a pingo filling could be interpreted as an increase in windspeed or a change in wind direction. Useful insights can be gathered by comparing the sand grain size distribution from the pie charts figures with the sand/silt ratio histograms because the two parameters are influenced by the same factors. The factors at play are the wind speed, direction and the availability of sediments. Interpreting the sand/silt ratio has limitations, such that wind direction cannot be accurately

reconstructed due to the inadequate quality of the sedimentary data found from the DINOloket database. Another aspect to why the wind direction is not straightforward to reconstruct is due to the fact that other external factors could also be at play such as changes in the sediment availability or changes in the sand/silt ratio within the same sediment source through time. Simply put, the results cannot prove changes occurring in the wind direction but can only indicate that it is a possible driver behind the fluctuations measured in the sand/silt ratio.

4.8.1 Syb

The odd case seen in Syb (Figures 26 & 31), consists of gradual sand homogenisation with a decline in grain size. If sand grain size decline and homogenisation were driven by a reduction in wind speed, we would find a relative increase in the silt proportion, thus a lower sand/silt ratio. Contrary to expectation, this ratio across the stratigraphy peaks at the shallowest sample measured at 228-229 cm depth. Such unexpected trend can happen due to a change in the wind direction, so the origin of the blown-in aeolian sediments changes accordingly, which can bring a different mixture of sand/silt. This is not necessarily evidence that the wind direction changed because other external factors not considered could also play a role such as changes in the sand/silt ratio within the source of aeolian sediments.
Throughout the Younger Dryas, the sand became finer and homogenised, yet poorer in silt. This contrasting observation makes it possible to speculate but not prove, that towards the end of the Younger Dryas, the seasonal wind direction may have changed independently to its speed. This would explain a decrease in sand median diameter despite the widely accepted fact that the wind intensity was gradually increasing, which would have normally brought this value up by including larger grains of sand within its aeolian transport load.

4.8.2 Ei Van Onnen

Ei Van Onnen (Fig. 27 & 33) demonstrates perfectly that the opposite scenario to Syb, may also occur. Here there are no indicators that wind direction was necessarily changing while the evidence indicates that windspeed became stronger with time.
Looking at samples from depths of 425-426 and 436-437 cm they respectively represent the end of the YD and the end of an intermediate return to higher organic content in the sediments. For these two particular samples, the shallower one is much more heterogeneous, containing greater proportions of medium and coarse sands while the deeper sample is relatively more homogenised towards the finer half of the extremely fine sands (75-53μm). The shallower sample (425-426 cm) indicates an extremely high sand/silt ratio (7:1) while the other sample (436-437 cm) is the sole case in the entire research that had a ratio >1, meaning that silt had a greater mass proportion than of sand.
The overall trend observed is one of heterogenization and coarsening of the aeolian sediments, in this case the most plausible explanation is a gradual increase through time of the wind speed which caused a wider range of sediment sizes to be transported into the pingo remnant.

4.8.3 Fraeylemaborg

In Fraeylemaborg (Fig 28 & 35), is found the highest sand/silt ratio, again located at the shallowest of the samples taken from the core. By comparing the sand/silt ratio trend with the

heterogeneity and sand median grain size for the 5 samples of this core, it is possible to make some insightful comments on the Younger Dryas climate progression.
Looking at the samples from deepest to shallowest, a few trends emerge. The first is that the sand starts quite heterogeneous in terms of grain size distribution. At shallower depth in the core the sands become slightly finer (from depth 497-498 cm towards 491-492 cm) and homogenised with an increase in silt proportion. This is possibly due to a decrease in wind speed which coincides with the increase in organic content at the intermediate peak seen in sample at the depth of 484-485 cm. Later the heterogeneity increases with a coarsening of the median grain size, indicating a potential increase in wind speeds. The weaker connection between the sand/silt ratio and the median grain size of the 2 deepest samples suggests that changes in aeolian deposit availability or wind direction changes may have occurred at the early stages of the YD. On the other hand, the stronger, linear correlation between sand/silt ratio and the median sand grain diameter in the later samples suggests that an increase in the wind speed may have occurred in the final stage of the Younger Dryas.

4.8.4 Veenklooster

Despite only having 2 samples taken, the Veenklooster pingo remnant (Fig.29 & 37) demonstrates the same general trend seen in the Fraeylemaborg and Ei Van Onnen sites. Through time, the median grain size of the aeolian sediments increased, supporting the hypothesis that the climate of the Younger Dryas climate became gradually windier, storms more common and the overall sandiness increased.
The two samples are extracted at 20 cm of stratigraphic depth from each other (180 and 200 cm) and display a slight trend of grain size heterogenization and coarsening of the sand distribution as shown in the pie charts. This trend coincides with an increment in sand/silt ratio and is likely caused by an increase in windspeed which has the force to transport a broader range of larger aeolian sediments.

5. Conclusion

Sediments dating back to the Younger Dryas stadial were cored from the filling of collapsed pingo remnants from the Northern Netherlands. The cores from 3 other pingo remnant fillings were also investigated in the study, for a total of 4 sites. The Loss on Ignition treatment on the sediments was used to reconstruct trends for the fluctuations in soil organic content throughout the Younger Dryas stage. From the LOI inorganic residuals of samples taken from the 4 cores, the sand and silt contents were fractionated with stacked sieves and liquid suspension, respectively. The fractionated portions were subdivided into 8 sand and 8 silt categories based on grain diameter intervals. Sediment distributions were calculated from the relative masses of the grain size categories for sands and silts at the depths from which the samples were taken from the 4 cores. The parameters measured were the changes in the sand median grain diameter, sediment grain size heterogeneity, Loss on Ignition residuals and the sand to silt ratio.

5.1 Aeolian Transport

The interpretation of the Younger Dryas sediments indicates that, given the predominant South-Westerly summer wind direction during the Younger Dryas stage, the aeolian sediment was

most available in Syb with 2 metres of Younger Dryas deposits, then Fraeylemaborg at 0.9 m and Veenklooster at 0.6 metres. The Ei Van Onnen site received the least amount of aeolian sediment throughout the Younger Dryas stage with just 24 cm of infill. The use of a database website (www.dinoloket.nl) that relies on third party coring work made the sediment comparisons sometimes incomplete or inadequate. More specifically, the third-party boreholes contained interpretations that sometimes conflicted with each other most likely due to the inaccuracy of subjective interpretations made on the field. It is better to conduct the interpretation of the sediments only after conducting sample treatments and measurements in the laboratory. In overall the inadequacy and inconsistency of the data available on DINOloket weakened the plausibility of the comparisons and interpretations conducted between the third-party data of the surrounding boreholes and the four ones that were investigated in this study.

5.2 Loss on Ignition

Through the Loss on Ignition treatment, it was found that the levels of organic content in the pingo fillings decreased during the Younger Dryas, reaching a peak low near the end of the stadial. This value hit 4% of organic content in two pingo cores (Ei Van Onnen & Fraeylemaborg) and 6% in the other pair (Syb & Veenklooster).
The interpretation of the LOI results for all sites indicate that the Younger Dryas progressed to a gradually colder, windier and stormier climate until its abrupt end. In 2 of the 4 cores, a moderate and short-lived peak in organic content was identified in the middle of the Younger Dryas.
Finally, in all sites except for Syb, the intensification of the wind and cold climate was reflected by sediments coarsening and undergoing heterogenization. All four sites experienced a distinctively stronger influx of aeolian sand than in the previous (Bølling–Allerød) and subsequent stadia (Holocene).

5.3 Interpretation of the Factors Combined

When there is a positive agreement between:

1) Sand/silt mass ratio.
2) Heterogeneity of the distribution of the sand grain diameter categories by mass.
3) Median sand grain diameter.

It could be interpreted as changes in the speed of the seasonal wind across long timescales. When the three parameters were found to be less correlated, such as in the case of the Syb pingo remnant site, the results could be interpreted as possible changes in the wind direction or in the sediment availability.

The takeaway from interpreting the sand/silt ratio with sand median grain diameter and LOI residual mass is that when these factors are in direct correlation, it is likely that wind speed is the parameter that is changing. When these factors have a weaker connection, it is likely that a multitude of other environmental and climatic factors are at play, like changes in vegetation density, wind direction, aeolian deposit composition and distribution.
When the sand categories, based on grain diameter, develop into a more heterogeneous mix, it is possible that the wind speed is increasing. When sand categories experience homogenisation and a reduction in median grain size, it is likely the wind speed that is decreasing.

For exception of Syb, the other three pingo cores contain sediments that suggest a gradual increase in wind direction throughout the YD, with a momentary hiatus in correlation with the intermediate peak consisting in a short-lived reversal to higher organic content in the sediment. The reason for why the sedimentation took place with a less predictable fashion in the Syb pingo does not have a single definitive answer and most likely is due to the compounding of several climatic and geomorphologic factors such as wind direction changes, storm events and aeolian sediment availability.

6. Appendix

6.1 Syb Microscope Photographs

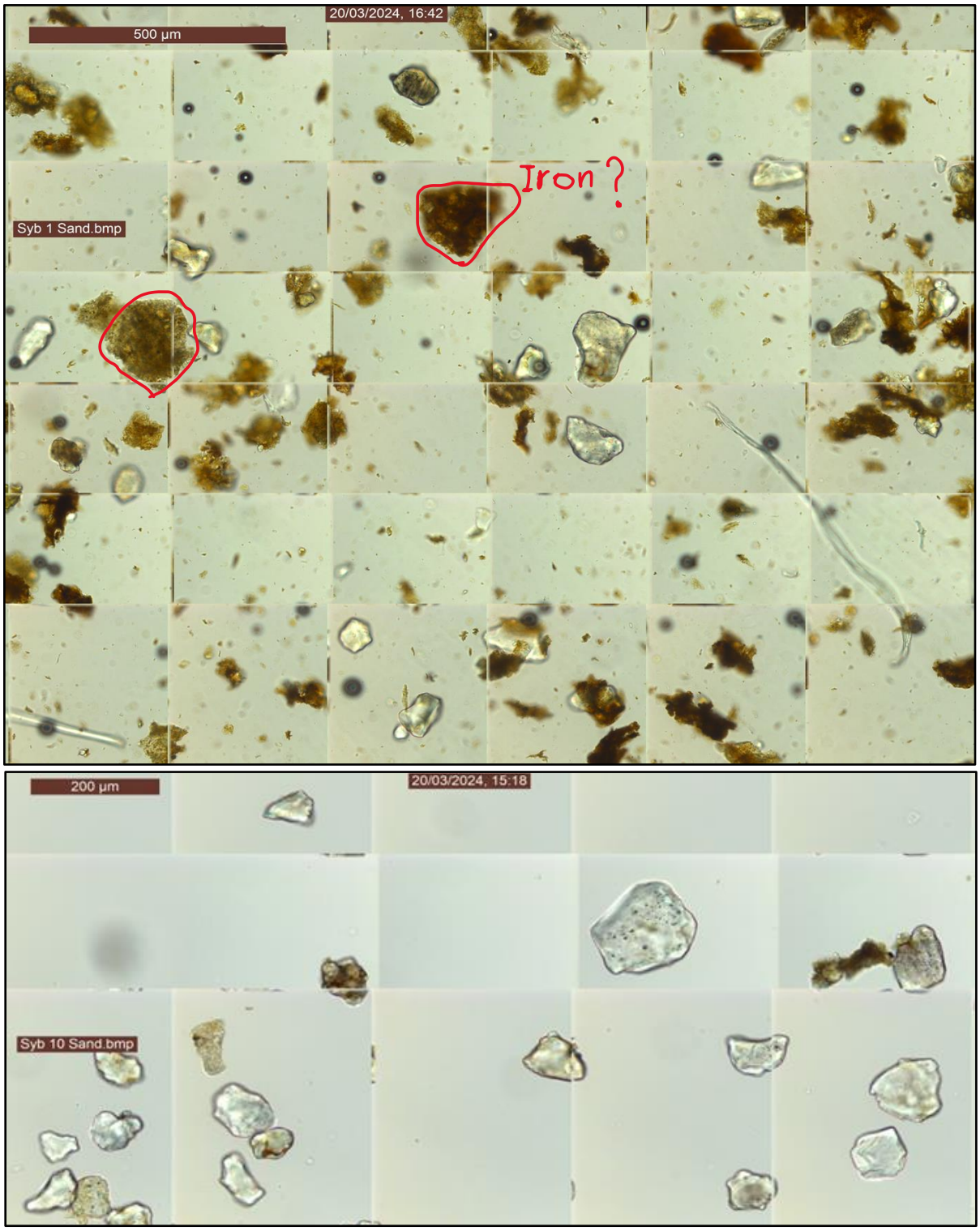

Figure 46 and 47. Show the microscope scans of the sand from the core at the Syb pingo remnant for respectively the deepest (418-419 cm) and the shallowest (228-229 cm) samples taken.

The most noticeable difference between figures 42 and 43 is the presence of smaller brown or yellow particles seen in the deeper section of the Syb core. Due to the temperatures of the

ashing process, any organic material is unlikely to have survived, and it is possible that those particles besides the sand may consist of sub-millimetre iron fragments. Despite this unusual presence, the size of the sand particles themselves appears similar and heterogeneous due to smaller and larger units.

6.2 Ei Van Onnen Microscope Photographs

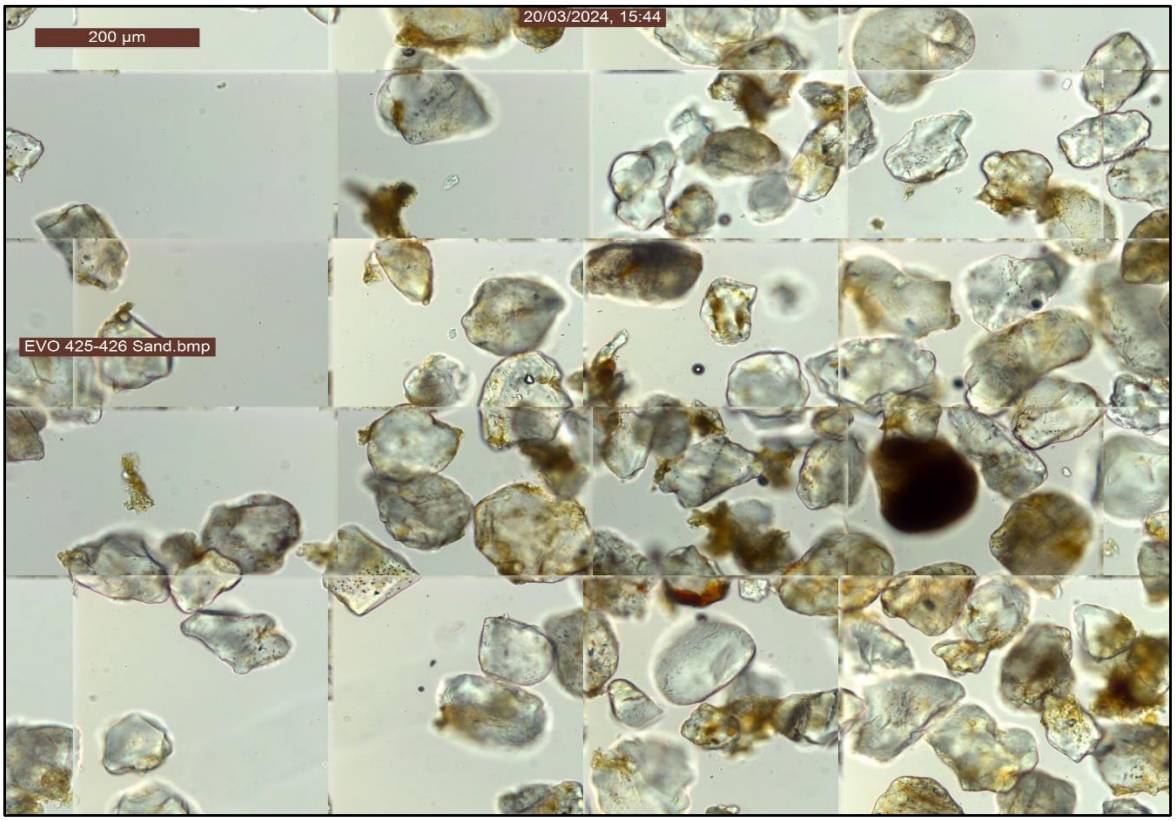

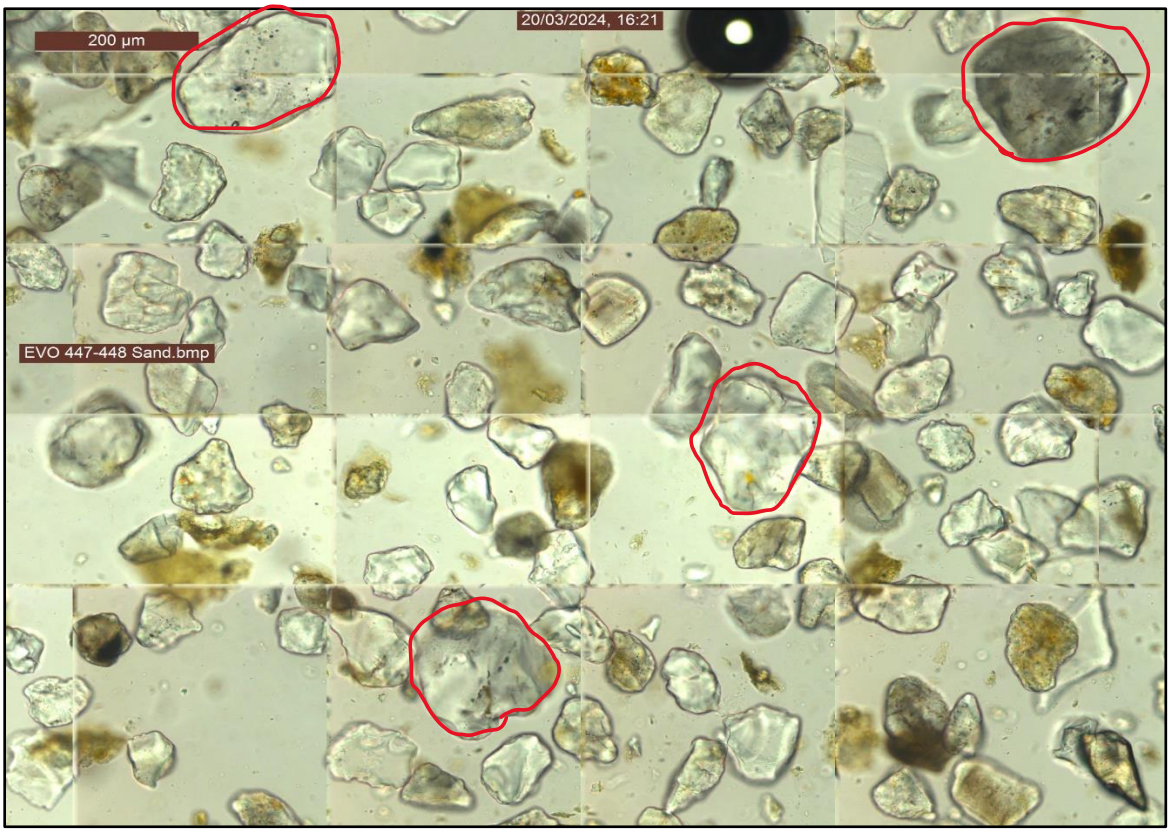

Figure 48 and 49. Show the microscope scans of the sand from the core at the Ei Van Onnen pingo remnant for respectively the deepest (447-448 cm) and the shallowest (425-426 cm) samples taken.

It is noticeable that the deepest sample (Fig.45) contains a few very large sand grains that have been circled in red, they are sometimes larger than the 200µm scale. It appears that the shallowest sample lacks the presence of such large sand grains (>200 µm) thus has a more homogeneous distribution of sand grains.

6.3 Fraeylemaborg Microscope Photographs

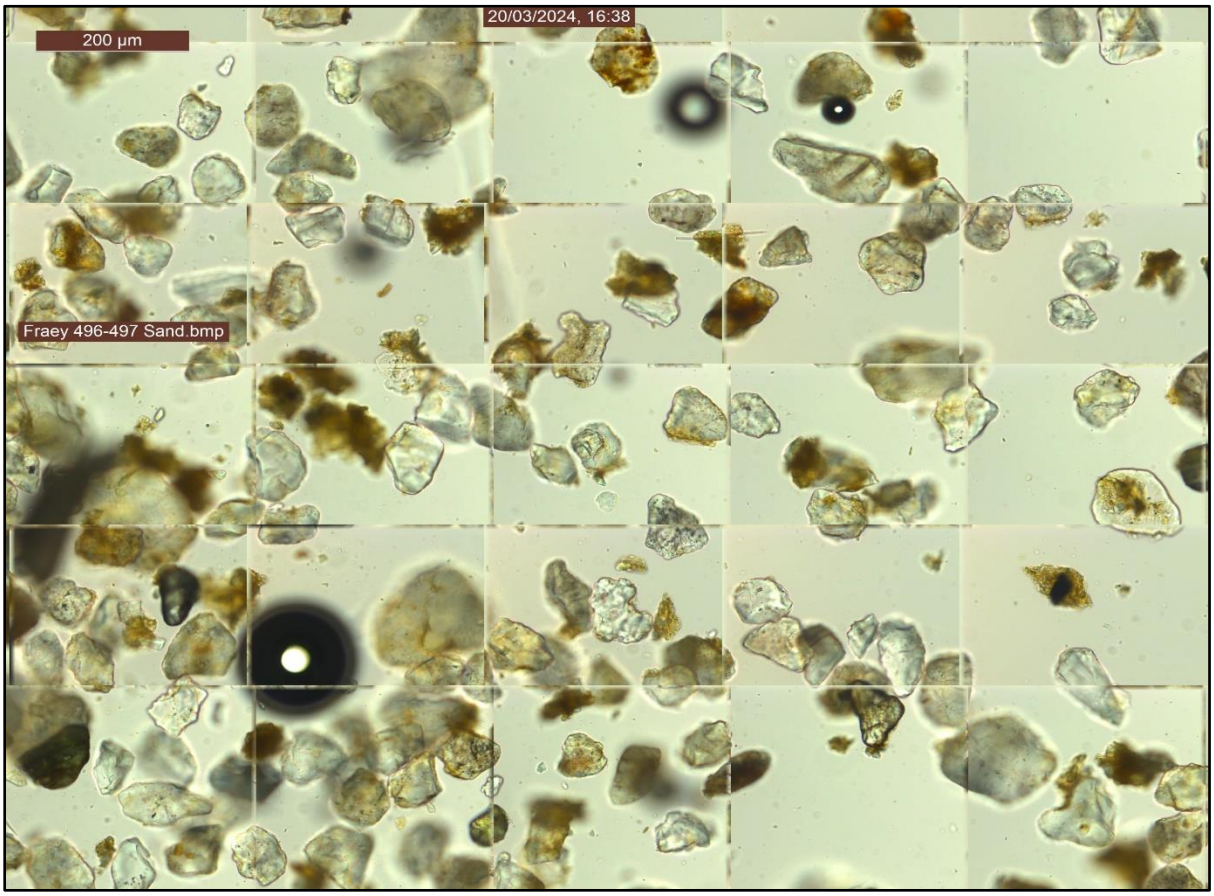

Figures 50 and 51 show the sand particles from respectively the shallowest (470-471 cm) to the deepest (496-497 cm) samples taken in Fraeylemaborg.

In the Fraeylemaborg pingo remnant, there are differences in the sand grains of these microscope images, the most prominent is the average grain size, noticeably superior in the shallower sample towards the end of the of the Younger Dryas. Another aspect is the homogeneity, the deepest sample (Fig.47) has a more limited range of grain diameters, while the shallowest sample (Fig.46) has a wider collection of grain sizes. The smaller sand grains in the 496-497 cm sample also exhibit sharper edges because the larger sand grains at 470-471 cm are generally more rounded.
We can interpret this stark contrast as part of the general trend that we have observed earlier with the sand/silt ratio, where the shallower samples in the Younger Dryas contain a more heterogeneous mix of sand types and the median diameter gradually becomes coarser.
On this occasion we witness under the microscope the same change that was measured in the lab, suggesting that wind speeds increased with time thus the aeolian sediments became coarser and heterogeneous.

6.4 Veenklooster Microscope Photographs

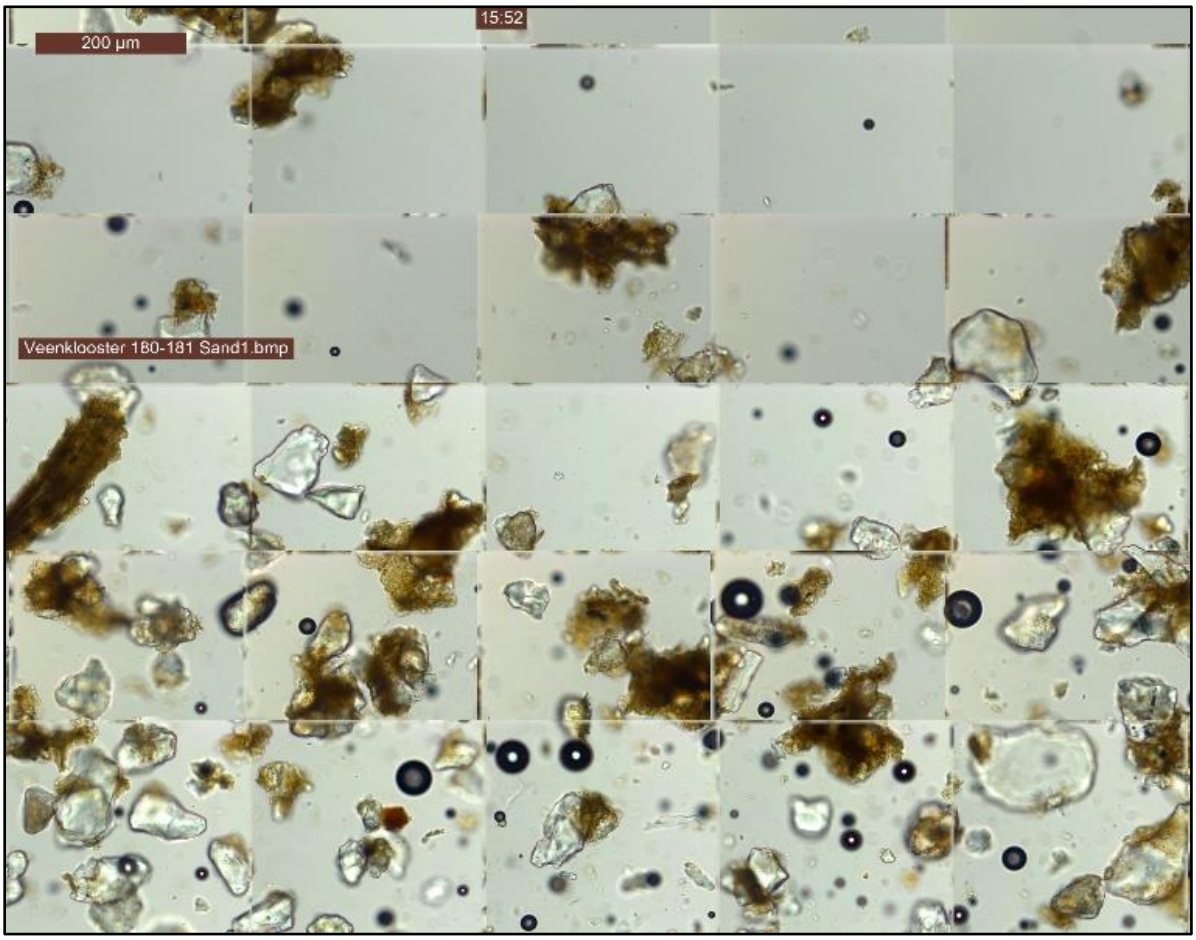

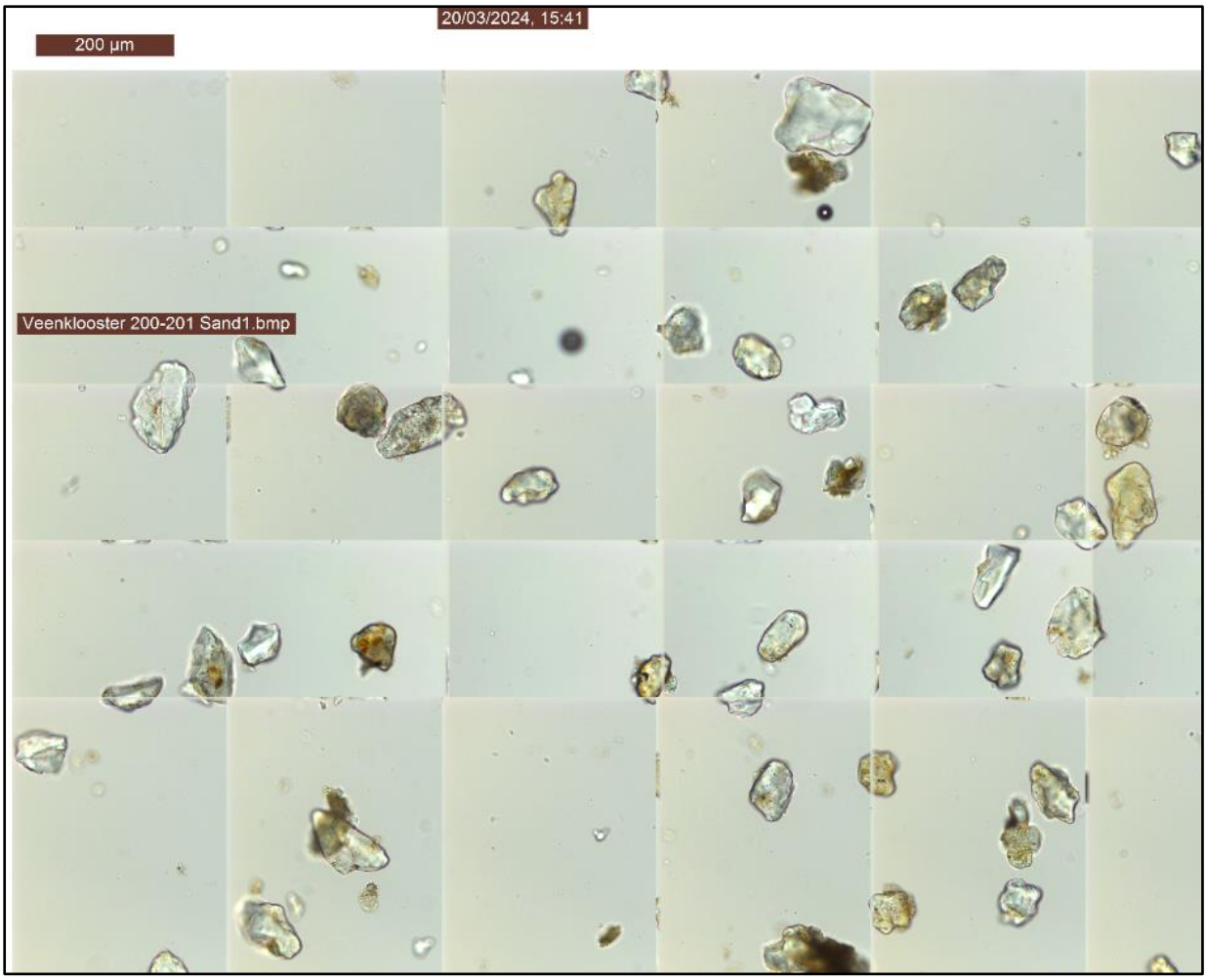

Figures 52 and 53 show the sand grains of the Veenklooster pingo core under the microscope for respectively the shallower (180-181 cm) and the deeper (200-201 cm) samples studied.

From the Veenklooster pingo, the first detail that distinguishes the two samples is the presence of more sub-millimetre fragments of what is possibly iron. The two samples have sand grains of similar roundness in the edges when compared with each other although the shallower sample (Fig.48) contains a higher proportion of very small sand particles, which contributes to its more heterogeneous composition and reflects the trend of heterogenization shown in the coloured pie chart figure 33.

8. Bibliography

Abbott, P.M., Niemeier, U., Timmreck, C., Riede, F., McConnell, J.R., Severi, M., Fischer, H., Svensson, A., Toohey, M., Reinig, F. and Sigl, M. (2021). Volcanic climate forcing preceding the inception of the Younger Dryas: Implications for tracing the Laacher See eruption. *Quaternary Science Reviews*, 274, p.107260. doi:https://doi.org/10.1016/j.quascirev.2021.107260.

AHN (n.d.). *AHN Viewer*. [online] AHN. Available at: https://www.ahn.nl/ahn-viewer.

Bazelmans, J., van Balen, R., Bos, J., Brinkkemper, O., Colenberg, J., Doeve, P., van Geel, B., Hakbijl, T., van Hateren, H., Hoek, W.Z., Huisman, H., Jansma, E., Kasse, C., van Os, B., van der Plicht, H., Schokker, J., Van der Putten, N. and van der Woude, J. (2021). Environmental changes in the late Allerød and early Younger Dryas in the Netherlands: a multiproxy high-resolution record from a site with two Pinus sylvestris populations. *Quaternary Science Reviews*, 272, p.107199. doi:https://doi.org/10.1016/j.quascirev.2021.107199.

Brauer, A., Haug, G.H., Dulski, P., Sigman, D.M. and Negendank, J.F.W. (2008). An abrupt wind shift in western Europe at the onset of the Younger Dryas cold period. *Nature Geoscience*, 1(8), pp.520–523. doi:https://doi.org/10.1038/ngeo263.

Broecker, W.S., Denton, G.H., Edwards, R.L., Cheng, H., Alley, R.B. and Putnam, A.E. (2010). Putting the Younger Dryas cold event into context. *Quaternary Science Reviews*, [online] 29(9-10), pp.1078–1081. doi:https://doi.org/10.1016/j.quascirev.2010.02.019.

Buizert, C., Gkinis, V., Severinghaus, J.P., He, F., Lecavalier, B.S., Kindler, P., Leuenberger, M., Carlson, A.E., Vinther, B., Masson-Delmotte, V., White, J.W.C., Liu, Z., Otto-Bliesner, B. and Brook, E.J. (2014). Greenland temperature response to climate forcing during the last deglaciation. *Science*, [online] 345(6201), pp.1177–1180. doi:https://doi.org/10.1126/science.1254961.

Cheng, H., Zhang, H., Spötl, C., Baker, J., Sinha, A., Li, H., Bartolomé, M., Moreno, A., Kathayat, G., Zhao, J., Dong, X., Li, Y., Ning, Y., Jia, X., Zong, B., Ait Brahim, Y., Pérez-Mejías, C., Cai, Y., Novello, V.F. and Cruz, F.W. (2020). Timing and structure of the Younger Dryas event and its underlying climate dynamics. *Proceedings of the National Academy of Sciences*, 117(38), pp.23408–23417. doi:https://doi.org/10.1073/pnas.2007869117.

Firestone, R.B., West, A., Kennett, J.P., Becker, L., Bunch, T.E., Revay, Z.S., Schultz, P.H., Belgya, T., Kennett, D.J., Erlandson, J.M., Dickenson, O.J., Goodyear, A.C., Harris, R.S., Howard, G.A., Kloosterman, J.B., Lechler, P., Mayewski, P.A., Montgomery, J., Poreda, R. and Darrah, T. (2007). Evidence for an extraterrestrial impact 12,900 years ago that contributed to the megafaunal

extinctions and the Younger Dryas cooling. *Proceedings of the National Academy of Sciences*, 104(41), pp.16016–16021. doi:https://doi.org/10.1073/pnas.0706977104.

Gea-Izquierdo, G., Montero, G. and Cañellas, I. (2009). Changes in limiting resources determine spatio-temporal variability in tree–grass interactions. *Agroforestry Systems*, 76(2), pp.375–387. doi:https://doi.org/10.1007/s10457-009-9211-4.

H. Renssen (2001). The climate in The Netherlands during the Younger Dryas and Preboreal: means and extremes obtained with an atmospheric general circulation model. *Netherlands Journal of Geosciences*, 80(2), pp.19–30. doi:https://doi.org/10.1017/s0016774600022289.

Heiri, O., Lotter, A.F. and Lemcke, G. (2001). Loss on ignition as a method for estimating organic and carbonate content in sediments: reproducibility and comparability of results. *Journal of Paleolimnology*, 25(1), pp.101–110. doi:https://doi.org/10.1023/A:1008119611481.

Hoek, W.Z. (1997). Late-glacial and early Holocene climatic events and chronology of vegetation development in the Netherlands. *Vegetation History and Archaeobotany*, 6(4), pp.197–213. doi:https://doi.org/10.1007/bf01370442.

Hoek, W.Z. and Bohncke, S.J.P. (2002). Climatic and environmental events over the Last Termination, as recorded in The Netherlands: a review. *Netherlands Journal of Geosciences - Geologie en Mijnbouw*, 81(1), pp.123–137. doi:https://doi.org/10.1017/s001677460002062x.

Hoek, W.Z. and Bos, J.A.A. (2018). The Allerød-Younger Dryas Transition: vegetation and geomorphological responses to rapid climate change in the Netherlands and surroundings. *Universiteit Utrecht (Archeo Projecten)*.

Hoek, W.Z., Donders, T.H., van Leeuwen, J., van Doorn, V., Schouten, S.J. and van Eijk, A.M. (2023). *14,700 years of climate and environmental change recorded in 17.8 meters of lake and peat deposits in the Nieuwe Veen pingo remnant near Hardenberg, NE Netherlands*. [online] Faculty of Geosciences Department of Physical Geography: Utrecht Universiteit. Available at: http://posters.geo.uu.nl/2023/14700_years_of_climate_and_environmental_change_recorded_in_17_8_meters_of_lake_and_peat_deposits_in_the_NieuweVeen_pingo_remnant_near_Hardenberg_NE_Netherlands-Hoek_Donders_vanLeeuwen_vanDoorn_Schouten_vanEijk-March2023.pdf [Accessed 18 Jun. 2024].

Holliday, V.T., Daulton, T.L., Bartlein, P.J., Boslough, M.B., Breslawski, R.P., Fisher, A., Jorgeson, I., Scott, A.C., Koeberl, C., Marlon, J.R., Severinghaus, J.P., Petaev, M.I. and Claeys, P. (2023).

Comprehensive refutation of the Younger Dryas Impact Hypothesis (YDIH). *Earth-Science Reviews*, pp.104502–104502. doi:https://doi.org/10.1016/j.earscirev.2023.104502.

Kasse, C., Woolderink, H.A.G., Kloos, M.E. and Hoek, W.Z. (2020). Source-bordering aeolian dune formation along the Scheldt River (southern Netherlands – northern Belgium) was caused by Younger Dryas cooling, high river gradient and southwesterly summer winds. *Netherlands Journal of Geosciences*, 99. doi:https://doi.org/10.1017/njg.2020.15.

Kluiving, S.J., Verbers, A.L.L.M. and Thijs, W.J.F. (2010). Lithological analysis of 45 presumed pingo remnants in the northern Netherlands (Friesland): substrate control and fill sequences. *Netherlands Journal of Geosciences - Geologie en Mijnbouw*, 89(1), pp.61–75. doi:https://doi.org/10.1017/s0016774600000822.

Kriek, M. (2015). *Younger Dryas Landscape (Twente) 10.000 BC*. *Mapping regional vegetation developments in Twente (the Netherlands) since the Late Glacial and evaluating contemporary settlement patterns, Netherlands Journal of Geosciences.* Available at: https://www.researchgate.net/figure/B-Artists-impression-of-the-landscape-in-the-Younger-Dryas-period-around-approximately_fig4_270816862 [Accessed 15 Jun. 2024]. BCL Archaeological Support.

Landschapsbeheer Drenthe (n.d.). *Pingoruïnes*. [online] Pingoruïnes. Available at: https://www.pingoruines.nl/pingoruines/ [Accessed 5 Apr. 2024].

Leshyk, V.O. (2018). *Why won't this debate about an ancient cold snap die?* [online] ScienceNews. Available at: https://www.sciencenews.org/article/younger-dryas-comet-impact-cold-snap.

Mackay, J.R. (2002). Pingo Growth and collapse, Tuktoyaktuk Peninsula Area, Western Arctic Coast, Canada: a long-term field study. *Géographie physique et Quaternaire*, 52(3), pp.271–323. doi:https://doi.org/10.7202/004847ar.

Mackay, J.R. (2011). Pingos of the Tuktoyaktuk Peninsula Area, Northwest Territories. *Géographie physique et Quaternaire*, 33(1), pp.3–61. doi:https://doi.org/10.7202/1000322ar.

Meissner, K.J. (2007). Younger Dryas: A data to model comparison to constrain the strength of the overturning circulation. *Geophysical Research Letters*, 34(21). doi:https://doi.org/10.1029/2007gl031304.

Murton, J.B., Bateman, M.D., Dallimore, S.R., Teller, J.T. and Yang, Z. (2010). Identification of Younger Dryas outburst flood path from Lake Agassiz to the Arctic Ocean. *Nature*, 464(7289), pp.740–743. doi:https://doi.org/10.1038/nature08954.

Péwé, T.L. (2024). *Permafrost - Surface manifestations of permafrost and seasonally frozen ground | Britannica*. [online] www.britannica.com. Available at: https://www.britannica.com/science/permafrost/Surface-manifestations-of-permafrost-and-seasonally-frozen-ground.

Pidwirny, M. (2006). *Periglacial Processes and Landforms". Fundamentals of Physical Geography, 2nd Edition.* [online] www.physicalgeography.net. Available at: http://www.physicalgeography.net/fundamentals/10ag.html.

Rasmussen, S.O., Andersen, K.K., Svensson, A.M., Steffensen, J.P., Vinther, B.M., Clausen, H.B., Siggaard-Andersen, M.-L. ., Johnsen, S.J., Larsen, L.B., Dahl-Jensen, D., Bigler, M., Röthlisberger, R., Fischer, H., Goto-Azuma, K., Hansson, M.E. and Ruth, U. (2006). A new Greenland ice core chronology for the last glacial termination. *Journal of Geophysical Research*, 111(D6). doi:https://doi.org/10.1029/2005jd006079.

Sir Horace Lamb (1945). *Hydrodynamics*. Courier Corporation.

Vivid Maps. (2018). *The Last Ice Age in Europe*. [online] Available at: https://vividmaps.com/last-ice-age-europe/ [Accessed 15 Jan. 2024].

Walker, M., Johnsen, S., Sune Olander Rasmussen, Popp, T., Steffensen, J.-P., Gibbard, P., Hoek, W. and Lowe, J. (2009). Formal definition and dating of the GSSP (Global Stratotype Section and Point) for the base of the Holocene using the Greenland NGRIP ice core, and selected auxiliary records. *Journal of Quaternary Science*, [online] 24(1), pp.3–17. doi:https://doi.org/10.1002/jqs.1227.

www.dinoloket.nl. (n.d.). *Formatie van Boxtel | DINOloket*. [online] Available at: https://www.dinoloket.nl/stratigrafische-nomenclator/formatie-van-boxtel [Accessed 4 Apr. 2024].

www.dinoloket.nl. (n.d.). *Ondergrondgegevens | DINOloket*. [online] Available at: https://www.dinoloket.nl/ondergrondgegevens.

Yoshikawa, K. (2013). Treatise on Geomorphology pages 274-297. *Elsevier eBooks*, 8, pp.274–297. doi:https://doi.org/10.1016/b978-0-12-374739-6.00212-8.